Journal of Visualized Experiments

Visualizing Lung Cellular Adaptations during Combined Ozone and LPS Induced Murine Acute Lung Injury
--Manuscript Draft--

Article Type:	Invited Methods Collection - Author Produced Video
Manuscript Number:	JoVE62097R2
Full Title:	Visualizing Lung Cellular Adaptations during Combined Ozone and LPS Induced Murine Acute Lung Injury
Corresponding Author:	Gurpreet Kaur Aulakh, PhD University of Saskatchewan Western College of Veterinary Medicine Saskatoon, Saskatchewan CANADA
Corresponding Author's Institution:	University of Saskatchewan Western College of Veterinary Medicine
Corresponding Author E-Mail:	gurpreet.aulakh@usask.ca
Order of Authors:	Jessica Andrea Brocos Duda
	Manpreet Kaur
	Gurpreet Kaur Kaur Aulakh, PhD

Additional Information:	
Question	Response
Please indicate whether this article will be Standard Access or Open Access.	Standard Access (US$1200)
Please confirm that you have read and agree to the terms and conditions of the author license agreement that applies below:	I agree to the Author License Agreement
Please specify the section of the submitted manuscript.	Immunology and Infection
Please indicate whether this article will be Standard Access or Open Access.	Standard Access ($1400)
Please provide any comments to the journal here.	

1 **TITLE:**
2 **Visualizing Lung Cellular Adaptations during Combined Ozone and LPS Induced Murine**
3 **Acute Lung Injury**
4

5 **AUTHORS:**
6 Jessica Andrea Brocos Duda[1], Manpreet Kaur[1], Gurpreet K. Aulakh[1]
7

8 [1]Small Animal Clinical Sciences, Western College of Veterinary Medicine, University of
9 Saskatchewan, Saskatoon, Canada
10

11 jab954@mail.usask.ca
12 m.kaur@usask.ca
13 gurpreet.aulakh@usask.ca
14

15 CORRESPONDING AUTHOR:
16 Gurpreet Kaur Aulakh
17

18 **KEYWORDS:**
19 Ozone, LPS, acute lung inflammation, F1F0 ATP synthase (complex V) subunits, immune
20 fluorescent cytology, IL-16
21

22 **SUMMARY:**
23 Combined ozone and bacterial endotoxin exposed mice show wide-spread cell death, including
24 that of neutrophils. We observed cellular adaptations such as disruption of cytoskeletal
25 lamellipodia, increased cellular expression of complex V ATP synthase subunit β and angiostatin
26 in broncho-alveolar lavage, suppression of the lung immune response and delayed neutrophil
27 recruitment.
28

29 **ABSTRACT:**
30 Lungs are continually faced with direct and indirect insults in the form of sterile (particles or
31 reactive toxins) and infectious (bacterial, viral or fungal) inflammatory conditions. An
32 overwhelming host response may result in compromised respiration and acute lung injury, which
33 is characterized by lung neutrophil recruitment as a result of the patho-logical host immune,
34 coagulative and tissue remodeling response. Sensitive microscopic methods to visualize and
35 quantify murine lung cellular adaptations, in response to low-dose (0.05 ppm) ozone, a potent
36 environmental pollutant in combination with bacterial lipopolysaccharide, a TLR4 agonist, are
37 crucial in order to understand the host inflammatory and repair mechanisms. We describe a
38 comprehensive fluorescent microscopic analysis of various lung and systemic body compartments,
39 namely the broncho-alveolar lavage fluid, lung vascular perfusate, left lung cryosections, and
40 sternal bone marrow perfusate. We show damage of alveolar macrophages, neutrophils, lung
41 parenchymal tissue, as well as bone marrow cells in correlation with a delayed (up to 36-72 h)
42 immune response that is marked by discrete chemokine gradients in the analyzed compartments.
43 In addition, we present lung extracellular matrix and cellular cytoskeletal interactions (actin,
44 tubulin), mitochondrial and reactive oxygen species, anti-coagulative plasminogen, its anti-
45 angiogenic peptide fragment angiostatin, the mitochondrial ATP synthase complex V subunits, α
46 and β. These surrogate markers, when supplemented with adequate *in vitro* cell-based assays and

47 *in vivo* animal imaging techniques such as intravital microscopy, can provide vital information
48 towards understanding the lung response to novel immunomodulatory agents.
49
INTRODUCTION:

51 Acute lung injury (ALI) is a crucial pathologic response of lungs to infectious or other harmful
52 stimuli which is marked by simultaneous activation of coagulative, fibrinolytic and innate immune
53 systems[1]. Neutrophils promptly sense microbial as well as intracellular damage patterns through
54 the Toll-like receptor (TLR) family[2-4]. Neutrophils release preformed cytokines and cytotoxic
55 granule contents, which can then cause collateral tissue damage. The ensuing alveolar damage is
56 marred with secondary cell death leading to release of molecules such as adenosine triphosphate
57 (ATP)[5], thus setting in a vicious cycle of immune-dysregulation.
58
59 An unsolved problem in the understanding of ALI relates to the question of how the injury is
60 initiated within the alveolar membrane. The electron transport complex V, F1F0 ATP synthase, is
61 a mitochondrial protein known to be expressed ubiquitously, on cell (including endothelial,
62 leukocyte, epithelial) plasma membrane during inflammation. The cell cytoskeleton which is
63 comprised of actin and tubulin, harbors many cell shape and function modulating as well as
64 mitochondrial proteins, respectively. We have recently shown that blockade of the ATP synthase
65 by an endogenous molecule, angiostatin, silences neutrophil recruitment, activation and
66 lipopolysaccharide (LPS) induced lung inflammation[6]. Thus, both biochemical (ATP synthase)
67 and immune (TLR4) mechanisms might regulate the alveolar barrier during lung inflammation.
68
69 Exposure to ozone (O_3), an environmental pollutant, impairs lung function, increases susceptibility
70 to pulmonary infections, and short low-levels of O_3 exposures increase the risk of mortality in
71 those with underlying cardiorespiratory conditions[7-14]. Thus, exposure to physiologically relevant
72 concentrations of O_3 provides a meaningful model of ALI to study fundamental mechanisms of
73 inflammation[7,8]. Our lab has recently established a murine model of low-dose O_3 induced ALI[15].
74 After performing a dose and time-response to low O_3 concentrations, we observed that exposure
75 to 0.05 ppm O_3 for 2 h, induces acute lung injury that is marked by lung ATP synthase complex V
76 subunit β (ATPβ) and angiostatin expression, similar to the LPS model. Intravital lung imaging
77 revealed disorganization of alveolar actin microfilaments indicating lung damage, and ablation of
78 alveolar septal reactive oxygen species (ROS) levels (indicating abrogation of baseline cell
79 signaling) and mitochondrial membrane potential (indicating acute cell death) after 2 h exposure
80 to 0.05 ppm O_3[15] which correlated with a heterogeneous lung [18]FDG retention[16], neutrophil
81 recruitment and cytokine release, most notably IL-16 and SDF-1α. The take-home message from
82 our recent studies is that O_3 produces exponentially high toxicity when exposed at concentrations
83 below the allowed limits of 0.063 ppm over 8 h (per day) for human exposure. Importantly, no
84 clear understanding exists on whether these sub-clinical O_3 exposures can modulate TLR4-
85 mediated mechanisms such as by bacterial endotoxin[17]. Thus, we studied a dual-hit O_3 and LPS
86 exposure model and observed the immune and non-immune cellular adaptations.
87
88 We describe a comprehensive fluorescent microscopic analysis of various lung and systemic body
89 compartments, namely the broncho-alveolar lavage fluid (i.e., BAL) which samples the alveolar
90 spaces, the lung vascular perfusate (i.e., LVP) that samples the pulmonary vasculature and the
91 alveolar septal interstitium in the event of a compromised endothelial barrier, left lung
92 cryosections, to look into resident parenchymal and adherent leukocytes left in the lavaged lung

93 tissue, peripheral blood which represents the circulating leukocytes and the sternal and femur bone
94 marrow perfusates that sample the proximal and distal sites of hematopoietic cell mobilization
95 during inflammation, respectively.
96
97 **PROTOCOL:**
98
99 The study design was approved by the University of Saskatchewan's Animal Research Ethics
100 Board and adhered to the Canadian Council on Animal Care guidelines for humane animal use.
101 Six-eight week old male C57BL/6J mice were procured. NOTE: Euthanize any animals which
102 develop severe lethargy, respiratory distress or other signs of severe distress before scheduled end
103 point.
104
105 NOTE: Prepare the following: 27-18 G needle-blunted (will depend on the mouse tracheal
106 diameter), appropriately sized PE tubing to fit the blunt needle (make a PE cannula for every
107 mouse), cannula, 2 sharp scissors, 2 blunt forceps (small), 1 sharp forceps (small), 3 1 mL syringes,
108 labelled microfuge tubes (for BAL, blood, vascular and bone marrow perfusate collection) and
109 labelled vials (for tissue fixation), sample bags/cryovials for tissue collection, butcher's cotton
110 thread roll (cut into adequate sized ligatures). All chemicals utilized for the experiments are
111 indicated in the **Table of Materials**.
112
113 1.   **Ozone and LPS exposures for induction of murine lung injury**
114
115 1.1.   Ozone exposure
116
117 1.1.1. Prepare a custom O_3 induction box. Add mouse feed, water bottle, enrichment toys and
118 clean bedding in order and mimic the mice' housing environment.
119
120 NOTE: These steps will ensure that the mice have free access to food and water when housed in
121 the custom induction box and will help alleviate undue stress.
122
123 1.1.2. Switch the O_3 calibrator/generator "ON" (placed towards the inlet port) to stabilize the UV
124 lamp before hand (around 15 min before exposures) and connect with in-line O_3 monitor.
125
126 NOTE: The O_3 monitor should read an average of 0.05 ppm, as sampled from the outlet at constant
127 chamber air temperature (72 $\pm$3 °F) and relative humidity (50$\pm$15%).
128
129 1.1.3. For O_3 exposures, gently place mice in the custom induction box and continuously expose
130 the mice to 0.05 ppm O_3 for 2 h.
131
132 1.2.   Anesthesia and intranasal LPS administration
133
134 1.2.1. Prepare 10 mg/mL stocks for ketamine and xylazine, separately.
135
136 1.2.2. Prepare a cocktail by mixing 20 parts of ketamine and 1 part of xylazine. If the mouse
137 weighs X g, inject (X/200) mL of ketamine/xylazine cocktail into the peritoneal cavity. For one

138 mouse, prepare 1 mL of cocktail comprising of 1000 µL of the 10 mg/mL ketamine stock and 50
139 µL of the xylazine stock. Mix well by pipetting up and down in a microfuge tube.
140
141 NOTE: The ketamine and xylazine stocks can be prepared a week in advance.
142
143 1.2.3. Anesthetize the mice under light intraperitoneal (IP) ketamine (50 mg/kg)/xylazine (1
144 mg/kg) mix (e.g., for a 25 g mouse, inject 0.125 mL of the cocktail).
145
146 1.2.4. Prepare a 1 mg/mL solution of LPS, in saline, and fill 50 µL of the solution in a pipette.
147
148 1.2.5. Hold the mouse upright with its back/dorsal side on the palm, holding the ears with the
149 same hand. Now, place 50 µL of the LPS solution[18] gently outside nostrils (i.e., 25 µL on each
150 nostril or 50 µL in one nostril; does not matter as long as the procedure is quick) and allow the
151 mice to inhale the LPS solution.
152
153 1.2.6. Instill control mice with 50 µL of sterile saline.
154
155 **Caution:** Do not exceed more than 100 µL for instillation, which could be fatal. Too less of a
156 volume (i.e., <50 µL) and there is risk of only nasal deposition.
157
158 1.2.7. Following LPS administration, gently lay down the mice, either on their stomach or their
159 back upon the mound of bedding with their head angled slightly downwards.
160
161 NOTE: This orientation prolongs retention of the solution in the nasal cavity[19].
162
163 1.2.8. At 0, 2, 4, 24, 36 and 72 h after the exposure, anesthetize the mice i.p. with full dose of
164 ketamine (200 mg/kg)/xylazine (4 mg/kg) mix (i.e., X/50 mL of the cocktail, where X is the mouse
165 weight in grams or 0.50 mL for a 25 g mouse).
166
167 1.2.9. Observe the mouse until it loses consciousness and the right reflex (i.e., does not turn back
168 when laid in supine position). Now, check the mouse for depth of anesthesia, by monitoring the
169 breathing (rhythmic chest excursions) and heart rate, which should fall noticeably, after 1-2
170 minutes.
171
172 1.2.10. Next, check for pedal reflexes i.e., pinch either of the hind-limb digits and observe for
173 retraction of the limb, as a reflex. If the mouse responds, top-up with additional 0.1 mL injections
174 or more, as required.
175
176 NOTE: To achieve deep anesthesia, bear in mind that certain strains or obese mice usually have a
177 larger volume of distribution and thus can be easily over-dosed, if sufficient time if not allowed
178 for full anesthesia (which can be around 10 minutes or more). Accordingly, some strains can be
179 resistant to anesthesia and thus require more top-ups. This knowledge is acquired after many
180 practical observations and experience with mice of different strains and age. As a few pilot
181 experiments were also performed immediately after O_3 and LPS exposures (i.e., at the 2 h time-
182 point), we also included some very early BAL cell analysis from those experiments to highlight
183 the immediate effects of the combined O_3 and LPS exposure.
184

185 **2.   Sample collection**
186
187 2.1.   Place the mouse on surgical tray. Now, gently put lubricating eye ointment on both the
188 eyes to avoid fluid loss and sanitize the mouse with 70% ethanol spray.
189
190 2.1.1.   Make small cuts through the upper and lower skin membranes with scissors, to expose the
191 trachea and thorax.
192
193 2.1.2.   Make a cut just below the sternum and expose the heart.
194
195 2.2.   Cardiac puncture
196
197 2.2.1.   Place a 25G needle attached to heparinized syringe into the right ventricle and draw blood
198 by cardiac puncture.
199
200 NOTE: Blood usually draws with minimal plunger draw, if the time from exposing the heart to
201 cardiac puncture is under a minute. After collecting around 0.4-0.5 mL, one may need to pause for
202 a few seconds before collecting the remaining blood. This is done to let the heart pump any
203 remaining volume into the right ventricular chamber. By the end of the blood collection, heart
204 stops to pump.
205
206 2.2.2.   Collect the blood and store in microfuge tubes for further processing.
207
208 2.3.   Tracheostomy
209
210 2.3.1.   Carefully use tweezers/blunt forceps to clear off the tracheal region from overlying tissue.
211 Use gloved hands more than the surgical instruments to avoid bleeding. If a lot of blood is oozing,
212 there is risk of contaminating the BAL samples. Use cotton swabs, if necessary, although not
213 preferred. Kimwipes are better alternatives.
214
215 2.3.2.   Now, cut through the ribcage to expose the lungs. Again, be **cautious** not to cut the sternum
216 and the intercostal arteries or the ascending aorta; make smaller cuts while advancing through the
217 rib cage)
218
219 2.3.3.   Pass a cotton ligature below the tracheal snip and leave as such for the time being.
220
221 2.3.4.   Snip the trachea at a suitable location in the distal 1/3rd portion, pointing towards the lungs,
222 to allow access for a 28 G tracheal cannula.
223
224 2.3.5.   Insert a 28 G PE cannula (a minimal length of 3-5 mm and distal end trimmed for ease of
225 insertion) into the trachea. Watch out for the end of the trachea before bifurcation and then pull
226 about a mm back to avoid sampling only single lobe.
227
228 2.3.6.   Firmly, tie cotton ligature to hold the cannula in place. Do not collapse the cannula.
229
230 2.4.   Broncho-alveolar lavage (BAL)
231

232   2.4.1. Fill 0.5 mL of PBS in a 1 mL syringe.

234   2.4.2. Now gradually inject 0.5 mL of PBS into the cannula with the help of 1 mL syringe.

236   2.4.3. After injecting PBS, aspirate out the syringe as long as it does not resist the suction.

238   NOTE: If there is resistance while aspirating the BAL fluid out, that indicates collapse of the
239   alveolar or bronchial tissue. In that case, pull back the cannula by a miniscule to detach the cannula
240   form the walls of the tissue.

242   2.4.4. Collect the aspirated fluid in a labelled microfuge tube and place on ice.

244   2.4.5. Perform two more lavages in similar fashion collecting in the same vial (i.e., a total of 0.5
245   X 3 = 1.5 mL lavage).

247   2.4.6. Measure the volume of collected BAL fluid. Lavage recovery should be close to 90%.

249   2.5.   Lung vascular perfusate (LVP)

251   2.5.1. Cut the descending thoracic aorta at a location between the thoracic and abdominal halves,
252   to avoid any back-up of perfusate in the lungs while perfusing through the right ventricle.

254   2.5.2. Blot the cavity near the cut aorta end, free of blood.

256   2.5.3. Next, perfuse the lungs with 0.5 mL of room-temp heparinized saline injected through the
257   right ventricle.

259   2.5.4. Collect the vascular perfusate from the cavity at the cut end of the descending thoracic
260   aorta, in a microfuge tube, placed on ice and measure its volume.

262   2.5.5. Ligate the right bronchus proximal to its branching from trachea (with cotton thread).

264   2.6.   In situ left lung fixation

266   2.6.1. Connect a 1 mL syringe to tracheal cannula, which is long enough to insert through the
267   previous tracheal incision.

269   2.6.2. Draw back air in the syringe up to 0.6 mL mark.

271   2.6.3. Then, fill the remaining syringe (up to the very end) with 2% paraformaldehyde at room
272   temperature. Make sure that the plunger is ready to pop out without sucking back any air from the
273   cannula.

275   2.6.4. Now, affix the syringe with a scotch tape, to an upright container, measured up to 20 cm
276   height.

278 2.6.5. Gently, draw the plunger out to let the fixative flow towards the trachea. In case there are
279 a few air bubbles in the cannula, gently place the plunger on top of the syringe and the fluid will
280 start to flow after a few seconds.
281
282 2.6.6. Let the left lung inflate to its total capacity in situ, for 5 minutes, from a 20 cm height
283 forming a 20 cm water column.
284
285 2.6.7. During this procedure, make sure to protect the right lung lobes from getting in contact
286 with paraformaldehyde as this will affect the downstream assays.
287
288 2.6.8. Place folded laboratory tissues to absorb any paraformaldehyde that might come in contact
289 with the right lung lobes.
290
291 Caution: Paraformaldehyde is highly toxic. Therefore, do not inhale or place contact to any
292 exposed parts of the body. Exercise extreme caution while handling.
293
294 2.6.9. During the time of paraformaldehyde instillation, sanitize the abdomen.
295
296 2.6.10. Cut the right lung lobes off from the trachea making sure to remove any thread and
297 immediately put the lobes in a labelled cryovial and drop it in liquid nitrogen for downstream
298 molecular/biochemical cytokine analysis/RT-PCR/western blot analysis of lung homogenate.
299
300 2.6.11. Carefully trim the left lung for any connective tissue or pleural membranes and dip it in
301 2% paraformaldehyde for 24 h at 4 $^{\circ}$ C.
302
303 2.6.12. Embed the fixed lung in paraffin as per standard embedding protocol.
304
305 **Caution:** Do not over-heat the lung samples.
306
307 2.6.13. Cut the abdominal part and de-skin it from the pelvic (hip) bone.
308
309 2.6.14. Separate out the left and right femur bones from the pelvic portion, in a saline filled petri
310 dish kept on ice.
311
312 2.7. Sternal and femur bone marrow aspirate collection
313
314 2.7.1. Clean the tissue and muscles off the bones by using laboratory tissues.
315
316 2.7.2. Collect the ventral ribcage and sternum into a saline filled Petri dish kept on ice.
317
318 2.7.3. Cut the distal and proximal tips of the sternal and femur bones.
319
320 2.7.4. Perfuse the bones 4 times with 0.5 mL of saline, using well-fitted needles (24 to 28 G) on
321 to 1 mL syringes, and collect the fractions from each bone into labelled tubes fitted with filters and
322 placed on ice.
323

324 NOTE: The needle gauge varies between animal size. After flushing, the femur bone should show
325 up transparent.
326
327 2.7.5. Once the samples have been collected, bag the mouse in a plastic bag and put in an animal
328 carcass freezer for proper disposal, as per guidelines of the institutional animal facility.
329
330 3.   **Sample processing**
331
332 3.1.   Total (TLC) and differential (DLC) leukocyte counts
333
334 3.1.1. Centrifuge peripheral blood, BAL, lung vascular perfusate and bone marrow (sternal and
335 femur) samples for 10 min at 500 g.
336
337 3.1.2. Collect the supernatants, flash freeze them and store them at -80 ⁰ C until further analysis.
338
339 3.1.3. Reconstitute the cells in a minimum of 200 μL of PBS.
340
341 3.1.4. Perform TLC by counting BAL, blood, lung vascular perfusate and bone marrow cells on
342 a hemocytometer.
343
344 3.1.5. Stain another 9 μL aliquot of BAL with a 1 μL mix of calcein green and red ethidium
345 homodimer-1 to quantify live (green) cells due to intracellular esterase activity and any damaged
346 BAL cells (in red) due to loss of plasma membrane integrity.
347
348 3.1.6. Add 2% acetic acid to lyse RBCs, in a 1:10 ratio for blood TLC and 1:2 ratio for lung
349 vascular perfusate TLC.
350
351 Caution: Adjust the cell concentrations by diluting in PBS if the concentration is more than $1x10^6$
352 cells per mL (very important for the bone marrow samples).
353
354 3.1.7. Centrifuge the cells to prepare cytospins on slides and stain as explained below for DLCs.
355 Count a minimum of 100 cells for differential leukocyte cell counts (DLCs).
356
357 NOTE: Typically, one can prepare two cytospins on one slide. And after 10-15 minutes of air
358 drying, proceed with staining step.
359
360 3.1.8. Split the collected BAL from three pilot mice per group into two cytospins each and stain
361 for actin/tubulin and mitochondria with active oxidative phosphorylation (reduced mitotracker).
362 Utilize the BAL from three more mice to split into two cytospins each, for NK1.1/Gr1/CX3CR1
363 and ATPβ/Ki-67/CD61/Angiostatin stained slides. Split the BAL from three more mice into two
364 cytospins each to stain for ATPα/Ly6G and CX3CR1/Siglec-F.
365
366 3.2.   Bronchoalveolar lavage (BAL) and Lung Vascular Perfusate (LVP) total protein
367 quantification
368

369 3.2.1. In order to quantify O_3 and LPS induced perturbations of the vascular barrier or the relative
370 oncotic pressure in the two pulmonary compartments (i.e., the alveolar septal (interstitial) and lung
371 vascular perfusate (vascular) compartments), measure total protein content in the collected fluids.
372
373 3.2.2. Analyze the thawed supernatant fractions for their total protein concentration using a
374 standard detergent resistant colorimetric assay.
375
376 3.3.   Bronchoalveolar lavage (BAL) and lung vascular perfusate (LVP) chemokine analysis
377
378 3.3.1. Next, analyze the chemokines in BAL and lung vascular perfusate (LVP) supernatants
379 using a 33-plex magnetic bead-based immunoassay. This will inform about the directionality of
380 airway/interstitium vs vascular chemokine gradients established after combined exposures.
381
382 3.3.2. Analyze the following panel of chemokines : CXCL13 (B-lymphocyte chemoattractant),
383 CCL27 (IL-11 R-alpha-locus chemokine (ILC)), CXCL5 (epithelial-derived neutrophil-
384 activating peptide 78 (ENA-78)), CCL-11 (eotaxin-1), eotaxin-2 (CCL-24), CX3CL1
385 (fractalkine), GM-CSF (CSF-2), CCL1, IFNγ (interferon gamma), IL-10 (interleukin-10), IL-16
386 (interleukin-16), IL-1β (interleukin-1 beta), IL-2 (interleukin-2), IL-4 (interleukin-4), IL-6
387 (interleukin-6), CXCL-10 (interferon gamma-induced protein 10 (IP-10)), CXCL11 (Interferon-
388 gamma-inducible protein 9 (IP-9)), KC (keratinocyte chemoattractant), MCP-1 (monocyte
389 chemoattractant protein-1), MCP-3 (monocyte chemoattractant protein-3), MCP-5 (monocyte
390 chemoattractant protein-5), MDC (macrophage-derived chemokine (CCL22)), MIP-1α
391 (macrophage inflammatory protein-1 alpha), MIP-1β (macrophage inflammatory protein-1 beta),
392 MIP-2 (macrophage inflammatory protein-2), MIP-3α (macrophage inflammatory protein-3
393 alpha), MIP-3β (macrophage inflammatory protein-3 beta), RANTES (regulated on activation,
394 normal T cell expressed and secreted (CCL5)), CXCL-16, CXCL-12/SDF-1alpha (stromal cell-
395 derived factor 1), TARC (thymus and activation regulated chemokine (TARC)), TECK (Thymus-
396 Expressed Chemokine (CCL25)) and TNFα (tumor necrosis factor alpha).
397
398 **4.   Cytospin staining and lung histology**
399
400 4.1.   Cytospin biochemical staining
401
402 4.1.1. Encircle the cytospins with a hydrophobic pen to contain the chemicals for incubation
403 during the procedure.
404
405 4.1.2. Rehydrate the cytospins in PBS for 5 minutes.
406
407 4.1.3. Fix the cytospin samples in 2% paraformaldehyde for 10 minutes, wash three times with
408 PBS for 5 minutes each.
409
410 4.1.4. Permeabilize with ice cold 70% acetone for 7 minutes and again wash three times with
411 PBS for 5 minutes each.
412

413 4.1.5. Stain for actin and tubulin or reduced Mitotracker (incubate with a mix of 2 µg/50 µL of
414 Alexa 488 conjugated phalloidin shown in green, and 2 µg/µL of Alexa 555 conjugated mouse
415 anti-α tubulin or reduced Mitotracker shown in red, respectively) for 15 minutes.
416
417 NOTE: Use mouse IgG1 isotype control antibody, in a separate cytospin, to validate the tubulin
418 staining protocol. Perform same steps as explained from 4.1.1 to 4.1.8, but for isotype controls.
419
420 4.1.6. Remove the stains by gently tipping the mix from the slide. Incubate the slides with DAPI
421 (4′,6-diamidino-2-phenylindole) for 5-10 min to stain nuclei.
422
423 4.1.7. Wash the cytospins 3 times with PBS for 5 min each, coverslip with anti-fade mounting
424 media and store overnight in dark at room temperature before imaging.
425
426 4.1.8. Acquire images under a wide-field upright microscope equipped with a scientific camera.
427 Ensure consistent camera exposure times set for the different fluorescent channels when imaging
428 slides.
429
430 **4.2.** ***Cytospin immune-fluorescent staining:***
431
432 4.2.1. Encircle the cytospins with a hydrophobic pen to contain the chemicals for incubation
433 during the procedure. Rehydrate the cytospins in PBS for 5 minutes.
434
435 4.2.2. Fix the cytospin samples by incubating in 2% paraformaldehyde for 10 minutes, wash three
436 times with PBS for 5 min each.
437
438 4.2.3. Permeabilize with 0.1% cold triton X-100 for 2 minutes, wash three times with PBS for 5
439 min each.
440
441 4.2.4. Next, Fc block for 15 minutes by incubating the cytospin with 1:50 dilution of the Fc block
442 antibody stock (to ensure that the primary mouse antibody does not cross-react non-specifically
443 with the mouse Fc antibodies).
444
445 4.2.5. Tip the slides to remove the Fc block and change to 1% BSA for and incubate the cytospin
446 with a mix of 3 primary antibodies of interest (refer to **Table 1** for the various combinations) for
447 30 minutes.
448
449 NOTE: Make sure to run isotype control antibodies (incubate with a mix mouse IgG1 and rat
450 IgG2b kappa primary antibodies by performing steps 4.2.1 to 4.2.9 and replacing the antibodies
451 with isotype controls) in parallel with corresponding secondary antibodies as discussed in our
452 recent study[20].
453
454 4.2.6. Wash 3 times with PBS for 5 min each. Incubate the cytospins with a mix of appropriately
455 designed secondary antibodies (please refer to **Table 1** for the details).
456
457 4.2.7. Remove the stains by gently tipping the mix from the slide, incubate with DAPI (4′,6-
458 diamidino-2-phenylindole) for 5-10 min to stain nuclei. Wash 3 times with PBS for 5 min each.

459

4.2.8. Coverslip with anti-fade mounting media and store overnight in dark at room temperature before imaging.

4.2.9. Acquire images under a wide-field upright microscope equipped with a scientific camera. Ensure consistent camera exposure times set for all the fluorophore channels when imaging slides.

4.3. Hematoxylin and eosin (H&E) histology

4.3.1. Perform modified H&E staining[3] on lung cryo-sections for all groups.

4.4. Image analysis

4.4.1. Process and analyze image data (.tiff) files in Fiji ImageJ open software (https://imagej.net/Fiji/Downloads).

4.4.2. Check the required parameters (Area, Perimeter, Integrated Density, Shape descriptors, Feret's diameter, Circularity, Display label) to be recorded under the **Analyze** tab and **Set Measurements**.

4.4.3. Using the **ROI manager**, manually outline around 50-200 cells in the merged image panel using the "freehand selections" tool. Save the regions of interest (ROI) with **Ctrl**+**T** command and copy the saved ROIs for each cell over to all the fluorophore channels.

4.4.4. Next press **Ctrl**+**M** to measure the pre-set parametersfor all the fluorescent channels (e.g., 405 nm (DAPI or ATPβ in blue), 488 nm (actin or NK1.1 or Ki-67 in green), 568 nm (tubulin or Gr1 or CD61 in red) and 633 nm (CX3CR1 or angiostatin in magenta)).

4.4.5. Save the Results as .csv file under an appropriate name that represents your analysis. Copy the Results from the .csv file over to a spreadsheet and divide the fluorescence intensity (FI) (which is the Raw Integrated Density column from the Results file) of the stained molecule by that of DAPI or CD61 FI, as per staining design. These ratios are termed as "DAPI or CD61 normalized FI ratios".

4.4.6. Next, plot these normalized ratios, circularity, cell perimeter and Feret diameter, to evaluate any change in cell size after the combined O_3 and LPS exposure.

4.4.7. Use appropriate statistical software to check the normality of the collected data and to test the null hypothesis (please refer to the statistical analysis section below).

4.5. Statistical Analysis

4.5.1. Express results as mean ± SEM. A minimum of three mice were used per group.

4.5.2. For chemokine data analysis, adjust one-way ANOVA p-values for false discovery rate according to the Benjamini and Hoshberg correction.

505

506 4.5.3. Analyze image parameters, cellularity, Feret diameter, perimeter, DAPI or CD61
507 normalized fluorescence intensity ratios by Mann-Whitney U test (for comparing two groups) or
508 Kruskal Wallis test (for comparing multiple groups) as these data were not normally distributed.
509

510 4.5.4. For rest of the imaging experiments, analyze the results using a one-way analysis of
511 variance followed by Sidak's multiple comparisons. p-values <0.05 were considered significant.
512

513 **REPRESENTATIVE RESULTS:**
514 ***Combined O_3 and LPS exposure leads to systemic inflammation and bone marrow mobilization***
515 ***at 72 h:*** Cell counts in different compartments revealed significant changes in peripheral blood
516 and the femur bone marrow total cell counts upon combined O_3 and LPS exposures. Although
517 combined O_3 and LPS exposures did not induce any changes in the total BAL (**Figure 1A**) or LVP
518 (**Figure 1B**) cell counts, polymorphonuclear cells presented as the predominant cell type at 24
519 (**Figure 1F, Supplemental Figure 1**), 36 and 72 h after exposure. Please note the absence of
520 Siglec-f and CX3CR1 staining in polymorphonuclear cells at 24 h BAL cytospin image (**Figure**
521 **1F**). Triple DAPI/CD11b/Gr1 staining of BAL cytospins showed presence of large CD11b- and
522 Gr1-positive mononuclear cells which are macrophages at 0 h, which changes to smaller
523 polymorphonuclear cells showing punctate Gr1staining but devoid of CD11b staining at 4 h (as
524 shown in the inset in **Supplemental 1F**). The majority of BAL cells are polymorphonuclear and
525 positive for both CD11b and Gr1, at 24 h post exposure (**Supplemental Figure 1**).
526

527 The mice displayed systemic leukocytosis at 24 h (3.3-fold vs 0 h, p<0.05, **Figure 1C**) followed
528 by leukopenia at 72 h which was marked by13-fold lower counts in peripheral blood compared to
529 24 h (p<0.01) and a 8.6-fold lower compared to 4 h (p<0.05) after combined O_3 and LPS exposure
530 (Figure 1C). The sternal bone marrow cells were also unchanged when compared to 0 h or after
531 combined O_3 and LPS exposure (**Figure 1D**). The femur bone marrow counts showed a late 28.8-
532 fold spike at 72 h when compared to 0 h (p<0.01, **Figure 1E**) as well as other time points (p<0.01,
533 **Figure 1E**). Visualization of the LVP, and sternal as well as femur bone marrow cells also showed
534 changes in the cell types to predominantly polymorphonuclear cells (**Supplemental Figure 1**).
535 The sternal bone marrow cells showed signs of damage as evidenced by extracellular nuclear
536 material. The femur bone marrow showed higher numbers of CD11b and Gr1 positive cells
537 (**Supplemental Figure 1**), which coincide with the cell counts.
538

539 ***BAL total protein content was highest at 36 h after combined O_3 and LPS exposure:***
540 Quantification of the total proteins in the LVP and BAL compartments was carried out to correlate
541 ozone induced lung edema i.e., plasma protein exudation due to resulting vascular and epithelial
542 barrier impairment due to the combined exposure. BAL total protein was 4.5-fold higher at 36 h
543 (p<0.05) when compared to 4 h (**Figure 2A**). However, LVP protein was unchanged after exposure
544 (**Figure 2B**).
545

546 ***Combined O_3 and LPS exposure induces strong chemokine gradients in the lung vascular***
547 ***compartment and not BAL:*** Chemokine multiplex assays were conducted on both BAL and LVP
548 supernatants. Please note that the relative differences between these two compartments represents
549 preferential retention in a particular compartment. The eosinophil chemoattractant eotaxin-2 was
550 4.3-fold higher at 4 h in the LVP compartment compared to 0 h (p<0.05, **Figure 3A**). In the BAL

compartment, eotaxin-2 was 3.2-fold lower at 4 h when compared to 0 h (p<0.01, **Figure 3B**). The BAL eotaxin-2 levels kept on decreasing consistently until 72 h with 12.6-fold reduction compared to 0 h (p<0.01, **Figure 3B**). The lymphocyte chemoattractant IL-2 was 10.1-fold higher at 4 h in the LVP compartment compared to 0 h (p<0.05, **Figure 3C**). In the BAL compartment, IL-2 was 5.0-fold lower at 36 h when compared to 0 h (p<0.05, **Figure 3D**). The BAL eotaxin-2 levels kept on decreasing consistently 5.9-fold reduction at 72 h compared to 0 h (p<0.05, **Figure 3D**).

Interestingly, many chemokines were altered at 4 h, in the LVP and not the BAL. Most of these chemokines showed modest, yet significant, increase in LVP levels at 4 h when compared to later time-points. Although eotaxin-1 levels were not high after the exposures when compared to 0 h, but the levels were significantly high at 4 h when compared to 24 (2.7-fold, p<0.05) and 72 h (5.0-fold, p<0.01, **Figure 4A**) after combined exposure. The levels of LVP TNFα were 3.4-fold higher at 4 h when compared to 36 h (p<0.05, **Figure 4B**). Similarly, LVP IFNγ was 2.9-fold higher at 4 h when compared to 72 h (p<0.05, **Figure 4C**). CX3CL1 levels were also high at 4 h when compared to 24 (1.7-fold, p<0.05), 36 (1.6-fold, p<0.05) and 72 h (2.2-fold, p<0.01) after combined exposures (**Figure 4D**). CCL27 levels showed higher levels at 4 h as well when compared to 24 (2.7-fold, p<0.05), 36 (3.9-fold, p<0.01) and 72 h (2.9-fold, p<0.05) after combined exposures (**Figure 4E**).

Some chemokines had a strong presence in the LVP at 4 h after combined exposures, and not changed in the BAL before and after exposure, , indicating a strong chemokine response from the pulmonary capillaries. At 4 h, IL-16 LVP levels were 3.4-fold compared to 0 h (p<0.01), 3.2-fold compared to 24 h (p<0.01), 4.5-fold compared to 36 h (p<0.01) and 4.6-fold compared to 72 h (p<0.01) after combined exposures (**Figure 4F**). At 4 h, the neutrophil chemokine, CXCL5 LVP levels were 2.0-fold compared to 0 h (p<0.01), 4.7-fold compared to 24 h (p<0.01), 2.2-fold compared to 36 h (p<0.01) and 2.7-fold compared to 72 h (p<0.01) after combined exposures (**Figure 4G**). At 4 h, CXCL10 LVP levels were 2.3-fold compared to 0 h (p<0.01), 2.1-fold compared to 24 h (p<0.05), 2.5-fold compared to 36 h (p<0.01) and 2.7-fold compared to 72 h (p<0.01) after combined exposures (**Figure 4H**). At 36 h, the neutrophil chemokine, SDF1α LVP levels were 4.2-fold compared to 0 h (p<0.01), 2.9-fold compared to 24 h (p<0.05), 6.8-fold compared to 72 h (p<0.01) after combined exposures (**Figure 4I**). At 4 h, MIP3β LVP levels were 2.3-fold compared to 0 h (p<0.05), and 2.3-fold compared to 72 h (p<0.05) after combined exposures (**Figure 4J**).

Combined O₃ and LPS exposure induces necrosis, disrupts cellular cytoskeletal, plasma membrane and mitochondrial integrity: As the compartmental leukocyte counts and protein contents were not correlating with the LVP chemokine gradients, it became more important to visualise the cells obtained from these compartments. *Ex vivo* actin/tubulin staining of baseline (0 h) BAL cells showed presence of cortical actin, stress fibers as well as lamellipodia (shown in green, **Figure 5** left upper panel) and microtubule network (shown in red, **Figure 5** left upper panel) that coincided with reduced mitotracker staining indicating presence of active mitochondria (shown in red, **Figure 5** left lower panel). More than 95% of the BAL cells were mononuclear at baseline. At 4 h, BAL cells showed extracellular nuclear material, punctate cytoplasmic actin staining devoid of lamellipodia and reduced cortical actin staining (shown in green, **Figure 5** right upper panel),fanned microtubule network (shown in red, **Figure 5** right upper panel) that did not correspond to the reduced mitotracker staining (shown in red, **Figure 5** left right panel). DAPI

normalized actin fluorescent intensity analysis showed a 3.7-fold decrease in the ratio indicating reduction in actin staining at 4 h after exposure (p<0.01, **Figure 6A**). Similarly, DAPI normalized tubulin fluorescent intensity also reduced by 1.5-fold after exposure (p<0.01, **Figure 6B**), indicating a reduction in tubulin staining. The loss of lamellipodia was evident with an increase in the circularity of BAL cellular cytoskeleton immediately i.e., at 2 h (p<0.01, **Figure 6C**) and 4 h (p<0.05, **Figure 6C**) after exposure when compared to 0 h and a decrease in the cytoskeletal circularity at 24 (p<0.05) and 36 h (p<0.01) after exposure, when compared to 0 h (**Figure 6C**).

Up to 24 h, the BAL cells from the combined exposure were double positive for calcein (in green, **Figure 7**) indicating presence of active esterase activity, and ethidium homodimer (in red, **Figure 7**), indicating that although some cells were dead (red), majority were partially compromised cells. At 36 h, the BAL cells were largely viable (green), indicating replacement of the compromised cells by leukocytes recruited from other systemic compartments (**Figure 7**).

Specific ATPα and Ly6G staining of the BAL cells revealed discrete intracellular localization (**Movies 1 and 2**) of both the proteins in alveolar macrophages as well as neutrophils after exposure (**Figure 7**). The combined exposure led to reduction in the DAPI normalized fluorescent intensity ratio of ATPα (**Figure 7, 8A**) and an increase in intracellular Ly6G protein content (**Figure 7, Figure 8B, Movies 1 and 2**). Reduction in ATPα staining, at 24 h after exposure, correlated with lower tubulin and to some extent reduced mitotracker staining. We also observed anuclear ATPα positive cell bodies after exposure, which could be platelets. However, we did not confirm our findings. At 2 h, we observed smaller mononuclear BAL cells (p<0.01 **Figure 8C**, p<0.01 **Figure 8D**) when compared to 0 h but at 4 h, the mononuclear cells were larger (p<0.01 **Figure 8C**, p<0.01 **Figure 8D**) when compared to 0 h. At 24 (p<0.01 Figure 8C, p<0.01 **Figure 8D**) and 36 h (p<0.01 **Figure 8C**, p<0.01 **Figure 8D**), the BAL cells became progressively smaller owing to a shift towards polymorphonuclear cells, when compared to 0 h.

Immunophenotyping of BAL cells revealed transient expressions of NK1.1, ATP β and Ki-67 and sustained expressions of Gr1, CX3CR1 and angiostatin positive BAL cells after combined O₃ and LPS exposures: Immunofluorescent staining of the first set of BAL cytospins were normalized to DAPI staining. There was an increase in the cellular NK1.1 positive cells at 24 h (p<0.05 vs 0 h, **Figure 9, 10A**). At 36 h, the BAL cells had lower cellular NK1.1 fluorescent intensity (p<0.01 vs 0 and 24 h, **Figure 9, 10A**). The cellular Gr1 fluorescent intensity was higher at 24 h (p<0.01 vs 0 h, **Figure 9, 10B**) as well as 36 h (p<0.01 vs 0 h, **Figure 9, 10B**). Similarly, the cellular CX3CR1 fluorescent intensity was higher at 24 h (p<0.01 vs 0 h, **Figure 9, 10C**) as well as 36 h (p<0.01 vs 0 h, **Figure 9, 10C**).

When normalized to cellular CD61, which is also ubiquitous in expression, revealed an increase in the cellular ATPβ fluorescent intensity at 24 h (p<0.01 vs 0 h, **Figure 9, 10D**) and a decrease in the cellular ATPβ fluorescent intensity at 36 h (p<0.01 vs 0 and 24 h, **Figure 9, 10D**). Notably, ATPβ showed predominantly nuclear localization at 24 h compared to peripheral localization at 36 h (**Figure 9**). The cellular fluorescent intensity of BAL Ki-67, an indicator of cellular proliferation, was higher at 24 h (p<0.01 vs 36 h, **Figure 9, 10E**) compared to 0 and 36 h. The levels were below baseline levels at 36 h (p<0.01, **Figure 9, 10E**), most likely due to higher polymorpho-nuclear CD61 vs Ki-67 expression at 36 h (**Figure 9**). Lastly, the cellular fluorescent intensity of BAL angiostatin was consistently high at both 24 and 36 h (p<0.01 vs 0 h, **Figure 9**,

10F), indicating a specific increase in this metalloproteinase cleaved plasminogen fragment, during the lung inflammatory response.

Combined exposures produce wide-spread lung damage: Lung histology revealed that the combined exposures produce prolonged damage to lungs as seen in H&E stained cryosections (**Figure 11**). Although bronchiolar and alveolar septal damage was expected, it was surprizing to observe endothelial damage of larger vessels, at 36 h after exposure (**Figure 11**). There were adherent intravascular leukocytes, patches of leukocyte aggregates (including neutrophils) in the damaged alveolar septal and peri-bronchiolar regions (**Figure 11**).

FIGURE LEGENDS:
Figure 1: Compartmental leukocyte counts: A) Broncho-alveolar lavage (BAL) total leukocyte counts at 0 (i.e., baseline), 4, 24, 36 and 72 h after combined 0.05 ppb ozone (O_3) and 50 μg intranasal LPS exposure to mice. **B)** Lung vascular perfusate (LVP) total leukocyte concentration at 0 (i.e., baseline), 4, 24, 36 and 72 h after combined 0.05 ppb ozone (O_3) and 50 μg intranasal LPS exposure to mice. **C)** Peripheral blood (PB) total leukocyte concentration at 0 (i.e., baseline), 4, 24, 36 and 72 h after combined 0.05 ppb ozone (O_3) and 50 μg intranasal LPS exposure to mice. **D)** Sternal bone marrow (BM) total leukocyte concentration at 0 (i.e., baseline), 4, 24, 36 and 72 h after combined 0.05 ppb ozone (O_3) and 50 μg intranasal LPS exposure to mice. **E)** Femur bone marrow (BM) total leukocyte concentration at 0 (i.e., baseline), 4, 24, 36 and 72 h after combined 0.05 ppb ozone (O_3) and 50 μg intranasal LPS exposure to mice. For the graphs A-E, 0 h is represented in blue, 4 h in red, 24 h in green, 36 h in purple and 72 h in orange data points; * $p<0.05$ and ** $p<0.01$**. F)** Representative BAL cytospin slide from 24 h exposure, showing mononuclear and polymorphonuclear cells when stained for nuclei with DAPI (in blue), CX3CR1 (in green) and Siglec-F (in red). Note that the merge of CX3CR1 and Siglec-F shows up as orange-yellow. Majority of mononuclear cells are positive for Siglec-F, which is a characteristic of alveolar macrophages. Scale bar = 50 μm.

Figure 2: Total Protein quantification: A) Bronchoalveolar lavage (BAL) total protein content and **B)** Lung vascular perfusate (LVP) total protein concentration was estimated by Pierce 660 nm protein assay (Thermoscientific, IL, US). For the graphs A-B, 0 h is represented in blue, 4 h in red, 24 h in green, 36 h in purple and 72 h in orange data points**;** * $p<0.05$.

Figure 3: Lung Eotaxin-2 and IL-2 chemokine gradients: Out of the 33 chemokines, two chemokines that were significantly altered in the lung vascular perfusate (LVP) and bronchoalveolar lavage (BAL) and fluid after combined 0.05 ppb ozone (O_3) and 50 μg intranasal LPS exposure to mice **A)** LVP eotaxin-2, **B)** BAL eotaxin-2, **C)** LVP IL-2 and **D)** BAL IL-2. Data were analyzed by one-way anova and the p-value for false discovery rate of multiple variables was adjusted as per Benjamini and Hoshberg correction. For the graphs A-D, 0 h is represented in blue, 4 h in red, 24 h in green, 36 h in purple and 72 h in orange data points. Pair-wise comparisons were analyzed after Bonferroni's correction. * represents $p<0.05$, ** represents $p<0.01$.

Figure 4: Lung vascular perfusate chemokine concentrations: Concentrations of ten more chemokines were altered, but only in the lung vascular perfusate (LVP) compartment. **A)** Eotaxin-1, **B)** TNFα, **C)** IFNγ, **D)** CX3CL1, **E)** CCL27, **F)** IL-16, **G)** CXCL5, **H)** CXCL10, **I)** SDF1α and **J)** MIP3β. For the graphs A-J, 0 h is represented in blue, 4 h in red, 24 h in green, 36 h in purple

689   and 72 h in orange data points. Pair-wise comparisons were analyzed after Bonferroni's correction.
690   * represents $p < 0.05$, ** represents $p < 0.01$.

691

692   **Figure 5: Bronchoalveolar lavage (BAL) cytospin actin/tubulin and reduced mitotracker**
693   **staining:** Representative images of actin/tubulin stained BAL cytospins from **A)** 0 h and **B)** 4 h
694   after combined 0.05 ppb ozone (O_3) and 50 µg intranasal LPS exposure to mice. Note that DAPI
695   is shown in blue, actin in green and tubulin in red. Representative images of reduced mitotracker
696   stained BAL cytospins from **A)** 0 h and **B)** 4 h after combined 0.05 ppb ozone (O_3) and 50 µg
697   intranasal LPS exposure to mice. Note that DAPI is shown in blue, and reduced mitotracker in red.
698   Scale bar = 50 µm.

699

700   **Figure 6: Bronchoalveolar lavage (BAL) cytoskeletal protein and circularity analysis:** BAL
701   cytospins stained for actin and tubulin were analyzed for DAPI normalized parameters i.e., **A)**
702   Actin to DAPI fluorescent intensity (FI) ratio at 0 and 4 h, **B)** Tubulin to DAPI fluorescent intensity
703   (FI) ratio at 0 and 4 h and **C)** BAL cell cellularity at 0 (n=75 cells), 2 (n=105 cells), 4 (n=66 cells),
704   24 (n=31 cells), 36 (n=154 cells) h. As a few pilot experiments were also performed immediately
705   after O_3 and LPS exposures i.e., at 2 h time-point, we also included some very early BAL
706   cellularity analysis from the 2 h time-point to highlight the immediate effects of O_3. For the graphs
707   A-C, 0 h is represented in blue, 2 h in red, 4 h in green, 24 h in purple and 36 h in orange data
708   points. * represents $p < 0.05$, ** represents $p < 0.01$.

709

710   **Figure 7: Bronchoalveolar lavage (BAL) intracellular and plasma membrane status:** BAL
711   cells were stained for vital stains, calcein (in green) and ethidium homodimers/EthHD (in red) as
712   shown in representative upper image panels at **A)** 0, **B)** 24 and **C)** 36 h after O_3 and LPS exposures.
713   Scale bar = 200 µm. BAL cytospins were immunostained for DAPI (in blue), ATPα (in green) and
714   Ly6G (in red). Representative images are shown in the lower image panels at **A)** 0 and **B)** 24 h
715   after O_3 and LPS exposures. Scale bar = 50 µm.

716

717   **Figure 8: Bronchoalveolar lavage (BAL) mitochondrial protein ATPα, lysosomal protein**
718   **Ly6G and cell size analysis:** Immunostained BAL cells were normalized for DAPI to compute
719   **A)** ATPα to DAPI fluorescent intensity (FI) ratio and **B)** Ly6G to DAPI FI ratio, at 0 and 24 h after
720   O_3 and LPS exposures. Immunostained BAL cells were also analyzed for their **A)** longest i.e.,
721   ferret diameter and **B)** perimeter, at 0, 2, 4, 24 and 36 h after O_3 and LPS exposures. For the graphs
722   A-D, 0 h (n=119 cells) is represented in blue, 2 h (n=105 cells) in red, 4 h (n=66 cells) in green,
723   24 h (n=309 cells) in purple and 36 h (n=154 cells) in orange data points. * represents $p < 0.05$, **
724   represents $p < 0.01$.

725

726   **Figure 9: Bronchoalveolar lavage (BAL) intracellular phenotyping:** BAL cells were
727   immunostained for DAPI (in blue), NK1.1 (in green), Gr1 (in red) and CX3CR1 (in magenta) as
728   shown in representative upper image panels at **A)** 0, **B)** 24 and **C)** 36 h after O_3 and LPS exposures.
729   Scale bar = 50 µm. BAL cytospins were immunostained for ATPβ (in blue), Ki-67 (in green),
730   CD61 (in red) and angiostatin (in magenta). Representative images are shown in the lower image
731   panels at **A)** 0, **B)** 24 and **C)** 36 h after O_3 and LPS exposures. Scale bar = 50 µm.

732

733   **Figure 10: Bronchoalveolar lavage (BAL) mitochondrial protein ATPβ, lysosomal protein**
734   **Gr1, intracellular CX3CR1 and angiostatin analysis:** Immunostained BAL cells were

735 normalized for DAPI to compute **A)** NK1.1 to DAPI fluorescent intensity (FI) ratio, **B)** Gr1 to
736 DAPI FI ratio and **C)** CX3CR1 to DAPI FI ratio, at 0, 24 and 36 h after O_3 and LPS exposures.
737 Immunostained BAL cells were normalized for CD61 to compute **A)** ATPβ to DAPI fluorescent
738 intensity (FI) ratio **B)** Ki-67 to DAPI FI ratio and **B)** Angiostatin (ANG) to DAPI FI ratio, at 0, 24
739 and 36 h after O_3 and LPS exposures. For the graphs A-F, 0 h (n=21 cells) is represented in blue,
740 24 h (n=796 cells) in red and 36 h (n=2692 cells) in green data points. * represents $p<0.05$, **
741 represents $p<0.01$.
742
743 **Figure 11: Lung hematoxylin and eosin (H&E) histology.** Ozone (O_3) and LPS induced lung
744 cryosection H&E histology at 0, 24 and 36 h after combined O_3 and LPS exposures. Regions of
745 alveolar epithelial damage are marked by solid black arrows and endothelial damage by black
746 arrow heads. Yellow asterisks (*) represent patches of leukocytes in the alveolar septal regions. **A**
747 = alveolar space, **B** = bronchus, **V** = vasculature, scale bar = 100 μm for left hand image panels
748 and 50 μm for image panels on the right side.
749
750 **Table 1:** Primary and secondary antibody combinations used to stain cytospins prepared from the
751 samples.
752
753 **Table 2:** A comprehensive summary of the main findings of the study in different compartments.
754 * denotes no change, + denotes an increase and − denotes a decrease in the measured parameters.
755 **BAL** denotes broncho-alveolar lavage fluid, **LVP** denotes lung vascular perfusate, **PB** denotes
756 peripheral blood, **SBM** denotes sternum bone marrow and **FBM** denotes femur bone marrow
757 compartment.
758
759 **Supplementary Figure 1: Gr1 and CD11b immunostaining:** Representative images from DAPI
760 (in blue), Gr1 (in green) and CD11b (in red) fluorescent immunostained cytospin slides of lung
761 vascular perfusate (LVP), sternal bone marrow (BM) and femur bone marrow (BM) compartments
762 at 0, 4 and 24 h after combined O_3 and LPS exposures. Scale bar = 50 μm.
763
764 **Supplementary Movie 1** Three-dimensional rendered volume of BAL macrophages from 0 h
765 time-point (i.e., baseline), showing nucleus (shown in blue) and immunostained for ATPα (shown
766 in green) and Ly6G (shown in red).
767
768 **Supplementary Movie 2:** Three-dimensional rendered volume of BAL macrophages from 24 h
769 time-point after combined O_3 and LPS exposures, showing nucleus (shown in blue) and
770 immunostained for ATPα (shown in green) and Ly6G (shown in red). Note the presence of
771 anuclear ATPα positive bodies as well as a fragmented cell.
772
773 **DISCUSSION:**
774 The methods presented in the current study highlight the usefulness of multiple compartment
775 analysis to study multiple cellular events during lung inflammation. We have summarized the
776 findings in **Table 2**. We and many labs have extensively studied the murine response to intranasal
777 LPS instillation, which is marked by rapid recruitment of lung neutrophils, which peaks between
778 6-24 h following which, resolution kicks in. And recently, we have shown that sub-clinical O_3 (at
779 0.05 ppm for 2 h) alone can induce significant lung damage in the C57BL/6NJ sub-strain[15], which
780 is marked by partitioning of neutrophils in the lung vascular compartment, while damaged

macrophages and debris were observed in the BAL, thus indicating the inflammatory potential of of O_3. In that model we observed an absence of neutrophils in the alveolar compartment as a result of O_3 induced alveolar epithelial damage and resulting phagocytosis by the alveolar macrophages. Not only did we observe extracellular DNA and debris in the O_3 model, the BAL macrophages were dysmorphic which correlate with high IL-16 levels, an alarmin usually released by dying neutrophils. Therefore, it is important to understand whether these sub-clinical O_3 levels can affect the immune response in otherwise robust C57BL/6J sub-strain, as noted with supra-physiological O_3 levels[21]. We observed that combined O_3 and intranasal bacterial endotoxin induced neutrophil recruitment in the pulmonary as well as systemic compartments, marked by presence of damaged neutrophils in BAL, lung vascular perfusate, sternal and femur bone marrow compartments starting at 4 h which remained high at 24, 36 and 72 h. The cellular damage was represented as loss of cortical actin and lamellipodia and increase in cell size in BAL leukocytes; neutrophils, analyzed in the BAL compartment, displayed significantly reduced positive reactivity to microtubule, ATP synthase complex V subunit α (ATPα) and active mitochondrial stain. Lungs adapt to this combined exposure by upregulating the expression of cellular ATP synthase complex V subunit β (ATPβ) as well as that of the ATPβ ligand, angiostatin (**Table 2**).

An important aspect of studying inflammation is to understand cellular necrosis along with chemokine gradients. It was interesting to note that the total leukocyte counts were not different except in peripheral blood and the femur bone marrow compartment. These observations led us to investigate the cellular cytoskeletal patterns, size and immunophenotyping. We observed a loss of lamellipodia and active mitochondria in BAL cells indicating cellular damage. Cortical actin organization is an essential feature of inter-cellular signaling and the resulting barrier properties. Cytoskeletal disorganization is thus a good marker of cell damage when necrosis is not as obvious to assess. Even at 36 h, the BAL cells had compromised plasma membrane as indicated by ethidium homodimer staining. Immediately after the combined exposures, neutrophils in BAL showed Gr1 positivity but an essentially negative staining for CD11b, which localizes towards the leading edge and aids in alveolar septal crawling[22]. Thus, the combined exposures lead to accumulation of atypical neutrophils devoid of the CD11b protein. LPS does not induce downregulation of CD11b. Thus, this feature is likely a result of O_3 induced damage to the neutrophils.

The BAL cells had a unique protein signature with higher NK1.1, Ki-67 and ATPβ staining at 24 h compared to 0 h (**Table 2**). The BAL cells had higher expression of Gr1, CX3CR1 as well as angiostatin, at 24 as well as 36 h when compared to 0 h (**Table 2**). These findings were corroborated by the presence of progressively more Gr1 positive neutrophils in BAL, at 24 and 36 h, after exposure (**Table 2**). The presence of NK1.1, CX3CR1 and Gr1 positive cells, at 24 h, indicates the recruitment of both mononuclear and polymorphonuclear cells in the BAL. Amongst the mononuclear cells, the CX3CR1 positive cells dominated at 36 h indicating presence of either interstitial macrophages, platelets or monocyte derived macrophages. The inclusion of both Ki-67 and angiostatin as markers informed us about the proliferative vs anti-angiogenic milieu, respectively in the BAL. Thus, the combined O_3 and LPS exposures lead to proliferation of probably macrophages followed by an anti-angiogenic milieu due to neutrophilic infiltration. The transient increase in ATPβ staining may indicate an important adaptation towards an increased survival of the BAL leukocytes at 24 h. It must be noted that ATPβ can bind to angiostatin and

826 inhibit prolonged survival[6,23], which is in fact reflected in the lower Ki-67 index at 36 h post
827 exposure.
828
829 Although BAL protein was highest at 36 h, and not other time-points, the lung vascular perfusate
830 did not show any changes in the protein concentration before or after exposure. It is possible that
831 the vascular compartment was not affected but this is most likely confounded due to oxidation of
832 electron-rich amino-acids such as methionine, histidine and cysteine by O_3 induced free radicals
833 and resultant surfactant proteins (SP-A, SP-B) degradation as well as vascular leak[24-26].
834 Quantification of BAL IgM, BAL surfactant proteins, BAL albumin or dye extravasation (using
835 Evans blue or fluorescein iso-thiocyanate (FITC) dextran) are alternative methods to assess
836 epithelial and endothelial integrity.
837
838 Interestingly, lung vascular perfusate levels of eotaxin-2 and IL-2 were acutely raised at the 4 h
839 time-point. BAL eotaxin-2 and IL-2 levels were significantly reduced after exposure, indicating
840 either degradation in the alveolar space or entrapment in the lung vasculature. More chemokines
841 analysed in lung vascular perfusate revealed higher levels of the eosinophil chemokine (eotaxin-
842 1), TNFα, IFNγ, lymph-node derived mononuclear cell chemokines (CX3CL1, CXCL10, CCL27,
843 MIP3β), epithelial derived neutrophil chemokine (CXCL5), and the alarmin (IL-16) released after
844 secondary necrosis of neutrophils[27], but only at 4 h after exposure. At 36 h, the bone marrow
845 derived pan-leukocyte chemokine, SDF1α[28], was higher in the lung vascular perfusate. The bone
846 marrow derived SDF1α concentrations correlate with cytology findings whereby CD11b and Gr1
847 positive cells are abundant at 24 and 36 h after exposure. Thus, the chemokine and cytological
848 profiles reflect significant leukocyte mobilization from the bone marrow compartments (Table 2).
849 Our animal model and research findings are vital keeping in mind the real world situations whereby
850 living beings in urban settings are likely exposed to such sub-clinical O_3 and infectious agents[8].
851 Our murine model serves as a readily accessible prototype that can be reproduced in level-2
852 containment labs for studying pulmonary and extra-pulmonary mechanisms of invasive cell death
853 and infections, as is case with COVID-19 infections[29]. Future studies should be directed at
854 visualizing the repair or late phase follow-up as well as chronic exposures to investigate the long-
855 term cellular adaptations. Thus, for comprehensive lung inflammation studies involving live
856 organ[15] and animal[16,30,31] imaging techniques, the current end-point study design can provide vital
857 insights into the host response to combined low-dose O_3 (cell death) and LPS (immune
858 stimulation), and thus deciphering the mechanisms of acute lung injury.
859

867

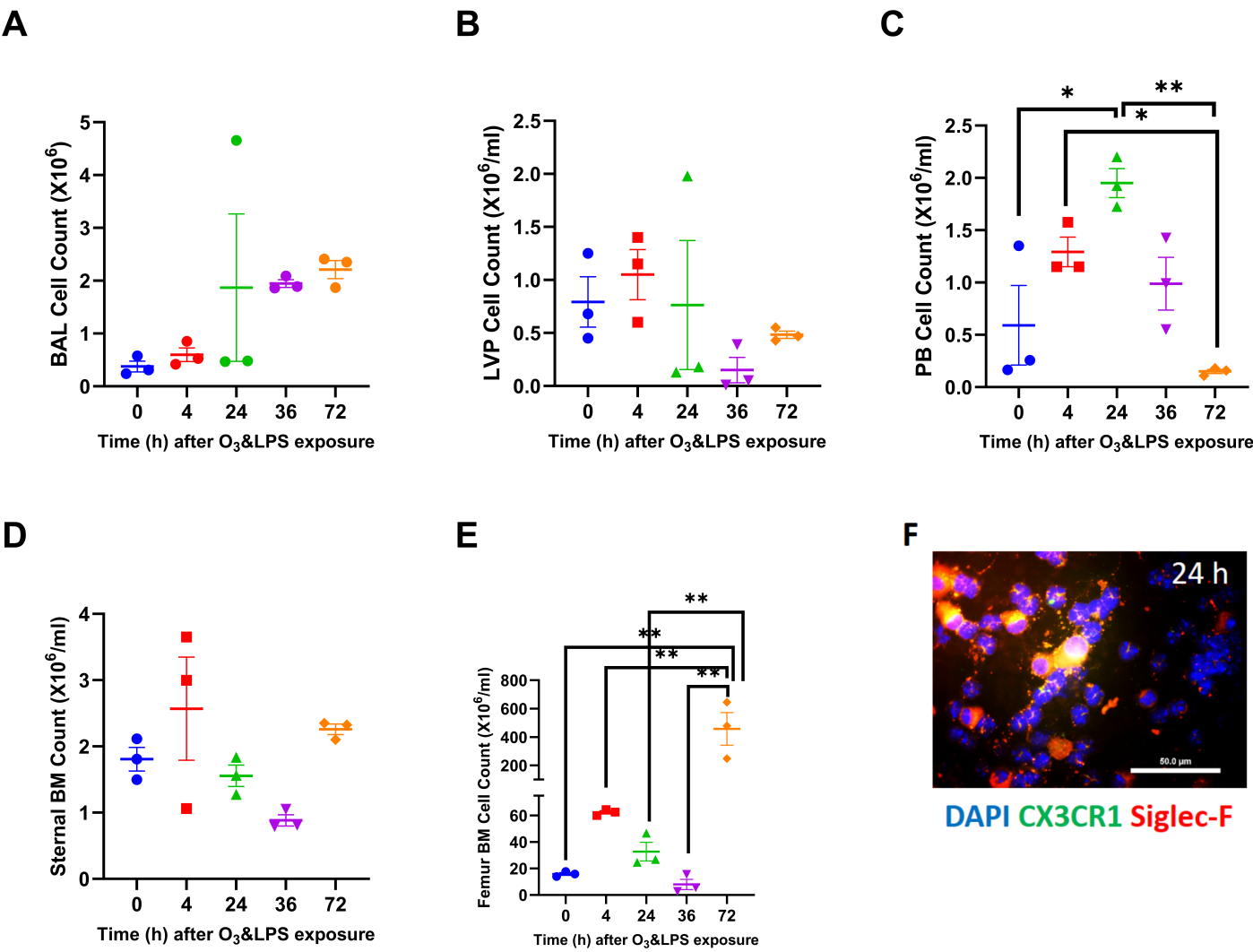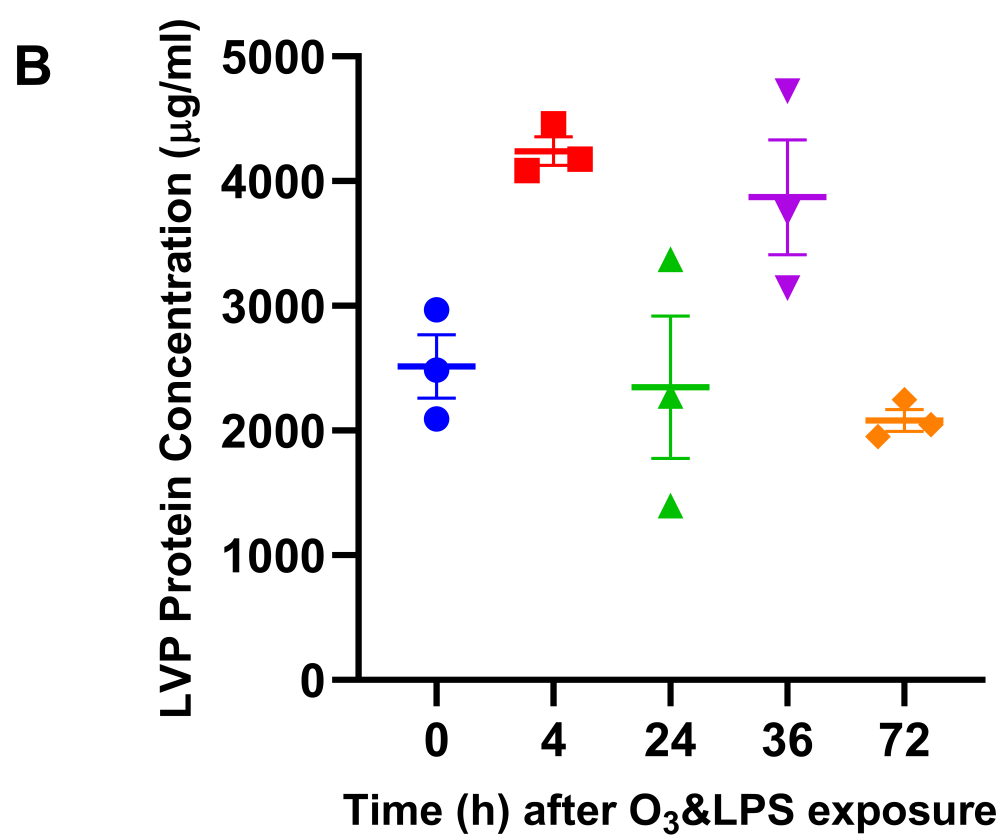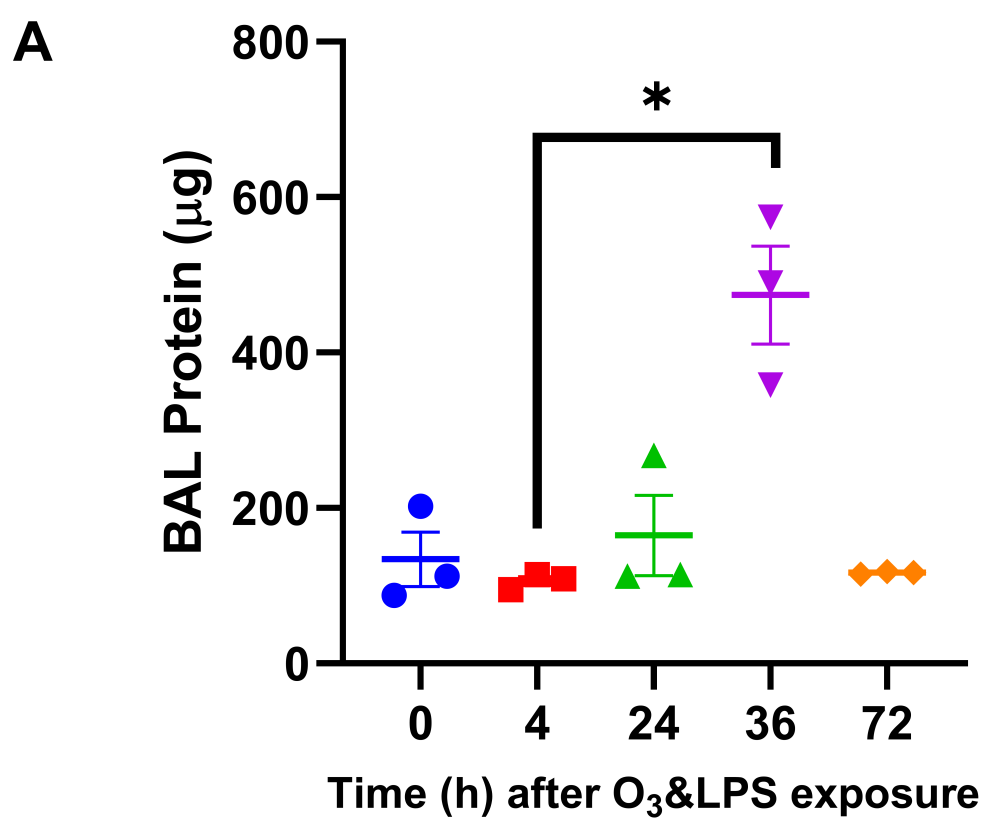868 **DISCLOSURES:**
869 The authors have no conflicts of interest or disclosures to make.
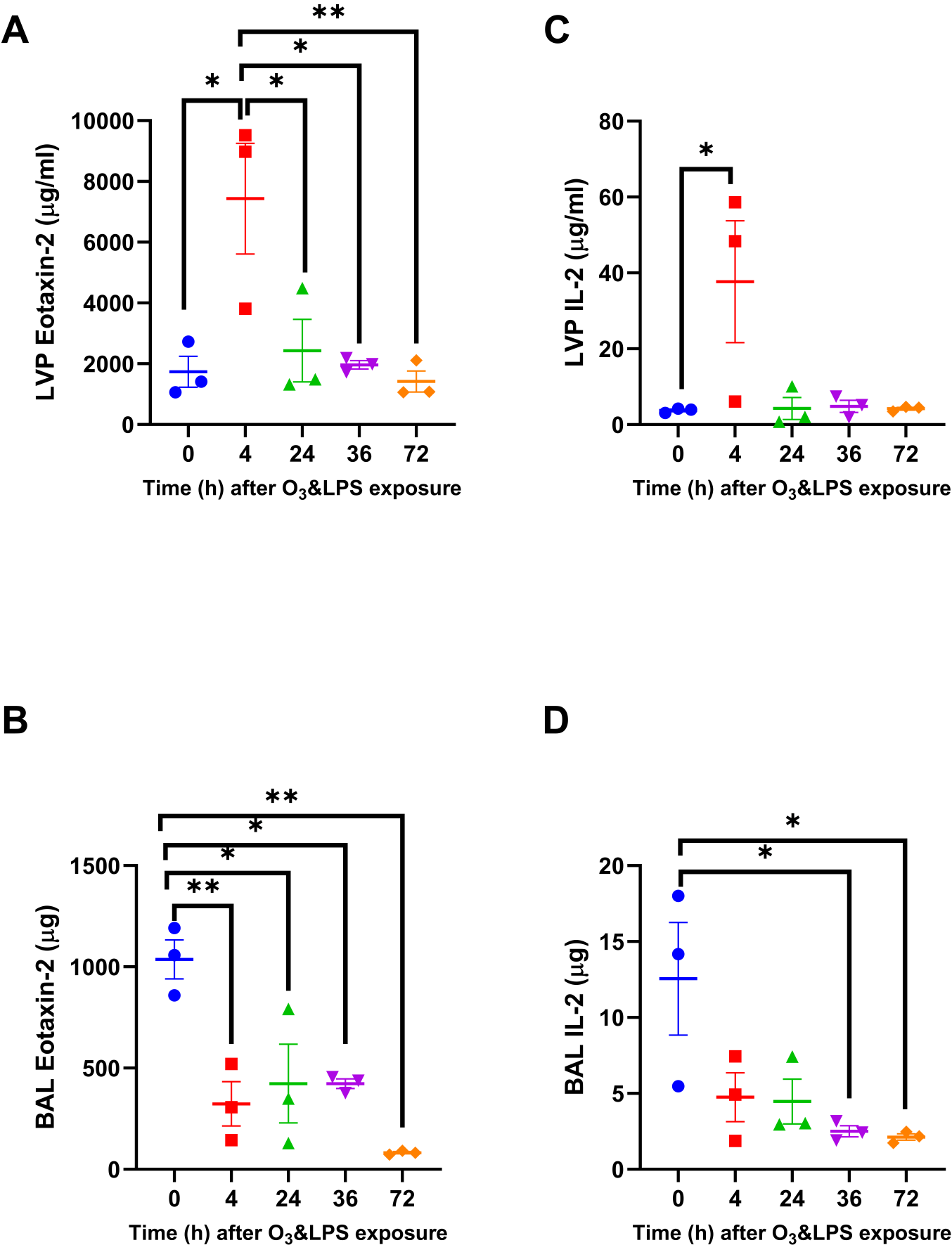870

871 **REFERENCES**

872   1   Bhattacharya, J., Matthay, M. A. Regulation and repair of the alveolar-capillary barrier in
873   acute lung injury. *Annual Review of Physiology.* **75**, 593-615 (2013).
874   2   Aulakh, G. K. Neutrophils in the lung: "the first responders". *Cell Tissue Research.*
875   10.1007/s00441-017-2748-z (2017).
876   3   Aulakh, G. K., Suri, S. S., Singh, B. Angiostatin inhibits acute lung injury in a mouse
877   model. *American Journal of Physiology - Lung Cellular and Molecular Physiology.* **306** (1),
878   L58-68 (2014).
879   4   Schneberger, D., Aulakh, G., Channabasappa, S., Singh, B. Toll-like receptor 9 partially
880   regulates lung inflammation induced following exposure to chicken barn air. *Journal of*
881   *Occupational Medicine and Toxicology.* **11** (1), 1-10 (2016).
882   5   Shah, D., Romero, F., Stafstrom, W., Duong, M., Summer, R. Extracellular ATP
883   mediates the late phase of neutrophil recruitment to the lung in murine models of acute lung
884   injury. *American Journal of Physiology - Lung Cellular and Molecular Physiology.* **306** (2),
885   L152-161 (2014).
886   6   Aulakh, G. K., Balachandran, Y., Liu, L., Singh, B. Angiostatin inhibits activation and
887   migration of neutrophils. *Cell Tissue Research.* 10.1007/s00441-013-1753-0 (2013).
888   7   Cakmak, S. et al. Associations between long-term PM2.5 and ozone exposure and
889   mortality in the Canadian Census Health and Environment Cohort (CANCHEC), by spatial
890   synoptic classification zone. *Environment International.* **111**, 200-211 (2018).
891   8   Dauchet, L. et al. Short-term exposure to air pollution: Associations with lung function
892   and inflammatory markers in non-smoking, healthy adults. *Environment International.* **121** (Pt
893   1), 610-619 (2018).
894   9   Delfino, R. J., Murphy-Moulton, A. M., Burnett, R. T., Brook, J. R., Becklake, M. R.
895   Effects of air pollution on emergency room visits for respiratory illnesses in Montreal, Quebec.
896   *American Journal of Respiratory and Critical Care Medicine.* **155** (2), 568-576 (1997).
897   10   Peterson, M. L., Harder, S., Rummo, N., House, D. Effect of ozone on leukocyte function
898   in exposed human subjects. *Environmental Research.* **15** (3), 485-493 (1978).
899   11   Rush, B. et al. Association between chronic exposure to air pollution and mortality in the
900   acute respiratory distress syndrome. *Environmental Pollution.* **224** 352-356 (2017).
901   12   Rush, B., Wiskar, K., Fruhstorfer, C., Celi, L. A., Walley, K. R. The Impact of Chronic
902   Ozone and Particulate Air Pollution on Mortality in Patients With Sepsis Across the United
903   States. *Journal of Intensive Care Medicine.* 10.1177/0885066618804497 885066618804497
904   (2018).
905   13   Stieb, D. M., Burnett, R. T., Beveridge, R. C., Brook, J. R. Association between ozone
906   and asthma emergency department visits in Saint John, New Brunswick, Canada. *Environmental*
907   *Health Perspectives.* **104** (12), 1354-1360 (1996).
908   14   Thomson, E. M., Pilon, S., Guenette, J., Williams, A., Holloway, A. C. Ozone modifies
909   the metabolic and endocrine response to glucose: Reproduction of effects with the stress
910   hormone corticosterone. *Toxicology and Applied Pharmacology.* **342**, 31-38 (2018).
911   15   Aulakh, G. K., Brocos Duda, J. A., Guerrero Soler, C. M., Snead, E., Singh, J.
912   Characterization of low-dose ozone-induced murine acute lung injury. *Physiological Reports.* **8**
913   (11), e14463 (2020).
914   16   Aulakh, G. K. et al. Quantification of regional murine ozone-induced lung inflammation
915   using [18F]F-FDG microPET/CT imaging. *Scientific Reports.* **10** (1), 15699 (2020).

917   17   Charavaryamath, C., Keet, T., Aulakh, G. K., Townsend, H. G., Singh, B. Lung
917   responses to secondary endotoxin challenge in rats exposed to pig barn air. *Journal of*
918   *Occupational Medicine and Toxicology (London, England).* **3**, 24-24 (2008).
919   18   Szarka, R. J., Wang, N., Gordon, L., Nation, P. N., Smith, R. H. A murine model of
920   pulmonary damage induced by lipopolysaccharide via intranasal instillation. *Journal of*
921   *Immunological Methods.* **202** (1), 49-57 (1997).
922   19   Southam, D. S., Dolovich, M., O'Byrne, P. M., Inman, M. D. Distribution of intranasal
923   instillations in mice: effects of volume, time, body position, and anesthesia. *American Journal of*
924   *Physiology - Lung Cellular and Molecular Physiology.* **282** (4), L833-839 (2002).
925   20   Aulakh, G. K. Lack of CD34 produces defects in platelets, microparticles, and lung
926   inflammation. *Cell Tissue Research* (2020).
927   21   Gilmour, M. I., Hmieleski, R. R., Stafford, E. A., Jakab, G. J. Suppression and recovery
928   of the alveolar macrophage phagocytic system during continuous exposure to 0.5 ppm ozone.
929   *Experimental Lung Research.* **17** (3), 547-558 (1991).
930   22   Yipp, B. G. et al. The Lung is a Host Defense Niche for Immediate Neutrophil-Mediated
931   Vascular Protection. *Science Immunology.* **2** (10) (2017).
932   23   Lee, T. Y. et al. Angiostatin regulates the expression of antiangiogenic and proapoptotic
933   pathways via targeted inhibition of mitochondrial proteins. *Blood.* **114** (9), 1987-1998 (2009).
934   24   Hawkins, C. L., Davies, M. J. Detection, identification, and quantification of oxidative
935   protein modifications. *Journal of Biological Chemistry.* **294** (51), 19683-19708 (2019).
936   25   Hemming, J. M. et al. Environmental Pollutant Ozone Causes Damage to Lung
937   Surfactant Protein B (SP-B). *Biochemistry.* **54** (33), 5185-5197 (2015).
938   26   Oosting, R. S. et al. Exposure of surfactant protein A to ozone in vitro and in vivo
939   impairs its interactions with alveolar cells. *American Journal of Physiology.* **262** (1 Pt 1), L63-68
940   (1992).
941   27   Roth, S. et al. Secondary necrotic neutrophils release interleukin-16C and macrophage
942   migration inhibitory factor from stores in the cytosol. *Cell Death & Discovery.* **1** 15056 (2015).
943   28   Kawaguchi, N., Zhang, T. T., Nakanishi, T. Involvement of CXCR4 in Normal and
944   Abnormal Development. *Cells.* **8** (2) (2019).
945   29   Gupta, A. et al. Extrapulmonary manifestations of COVID-19. *Nature Medicine.* **26** (7),
946   1017-1032 (2020).
947   30   Aulakh, G. K., Kuebler, W. M., Singh, B., Chapman, D. in *2017 IEEE Nuclear Science*
948   *Symposium and Medical Imaging Conference (NSS/MIC).* 1-2.
949   31   Aulakh, G. K. et al. Multiple image x-radiography for functional lung imaging. *Physics in*
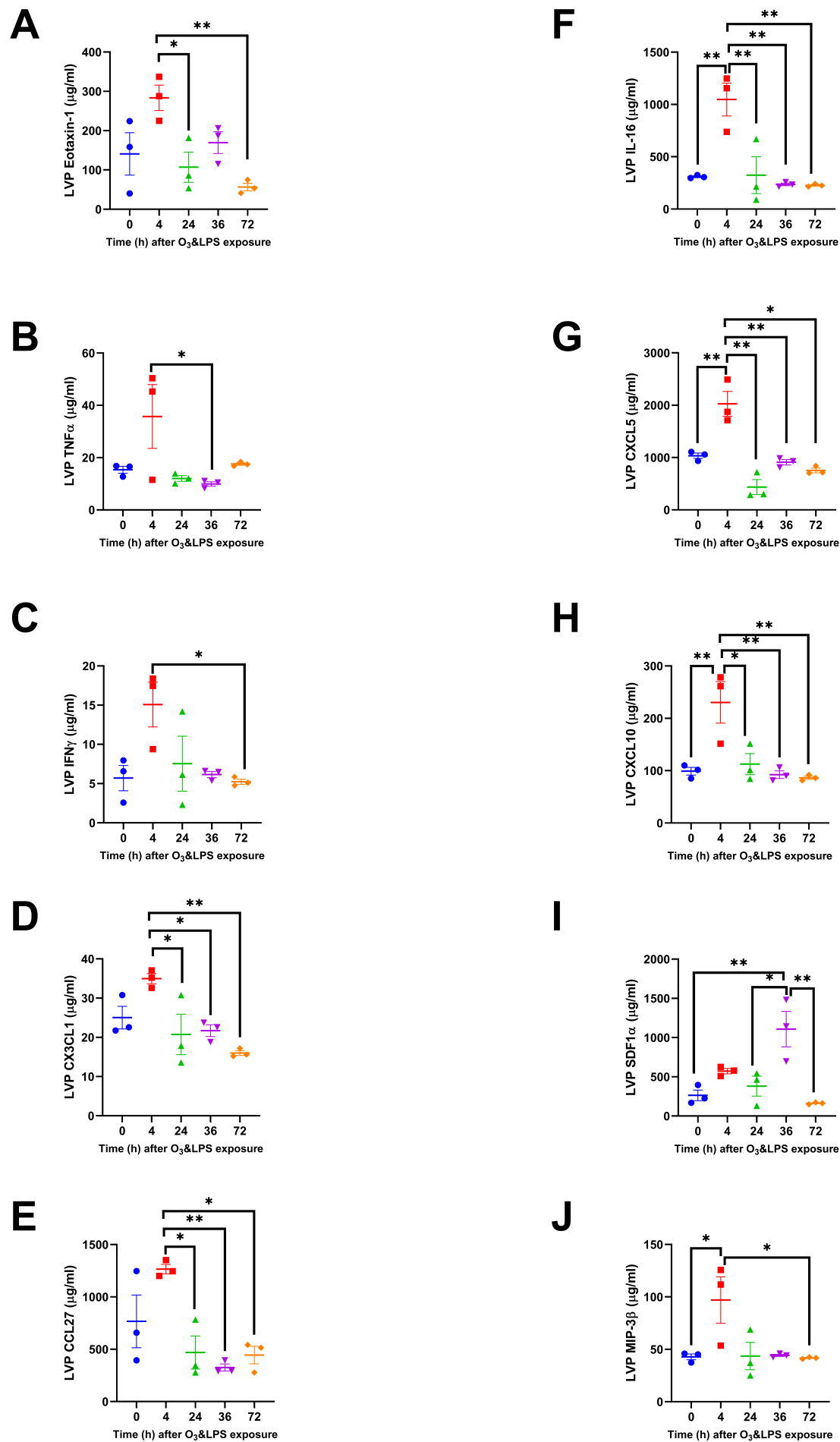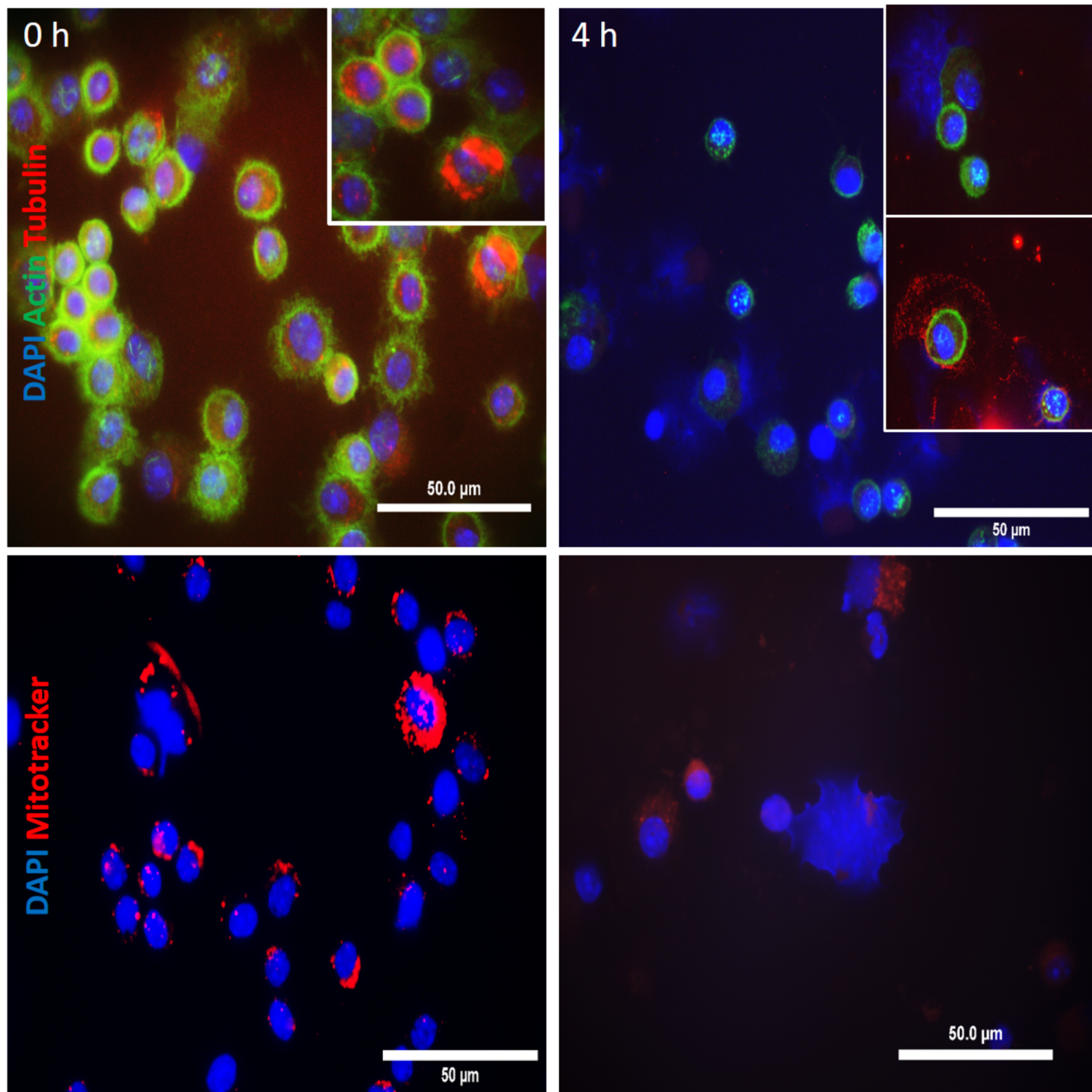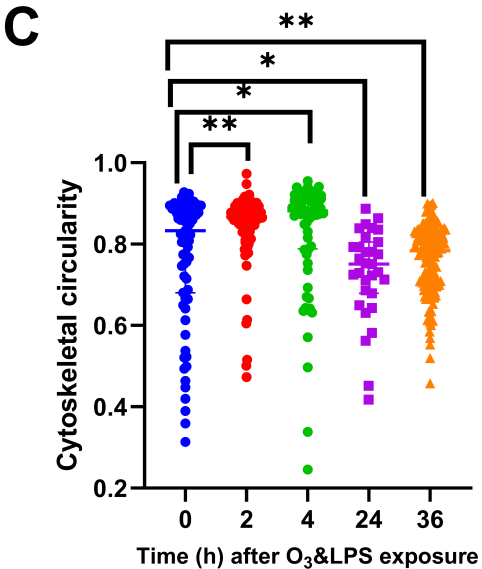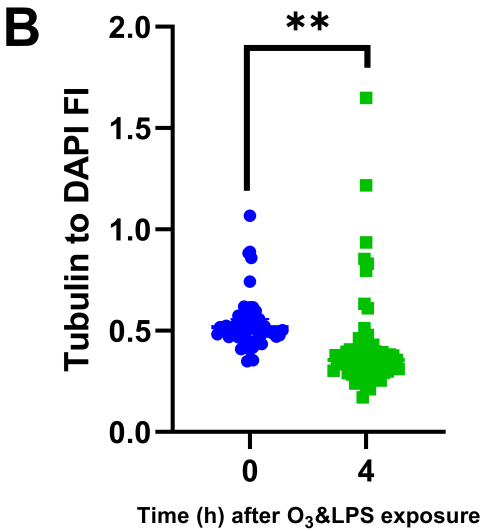950   *Medicine & Biology.* **63** (1), 015009 (2018).
951
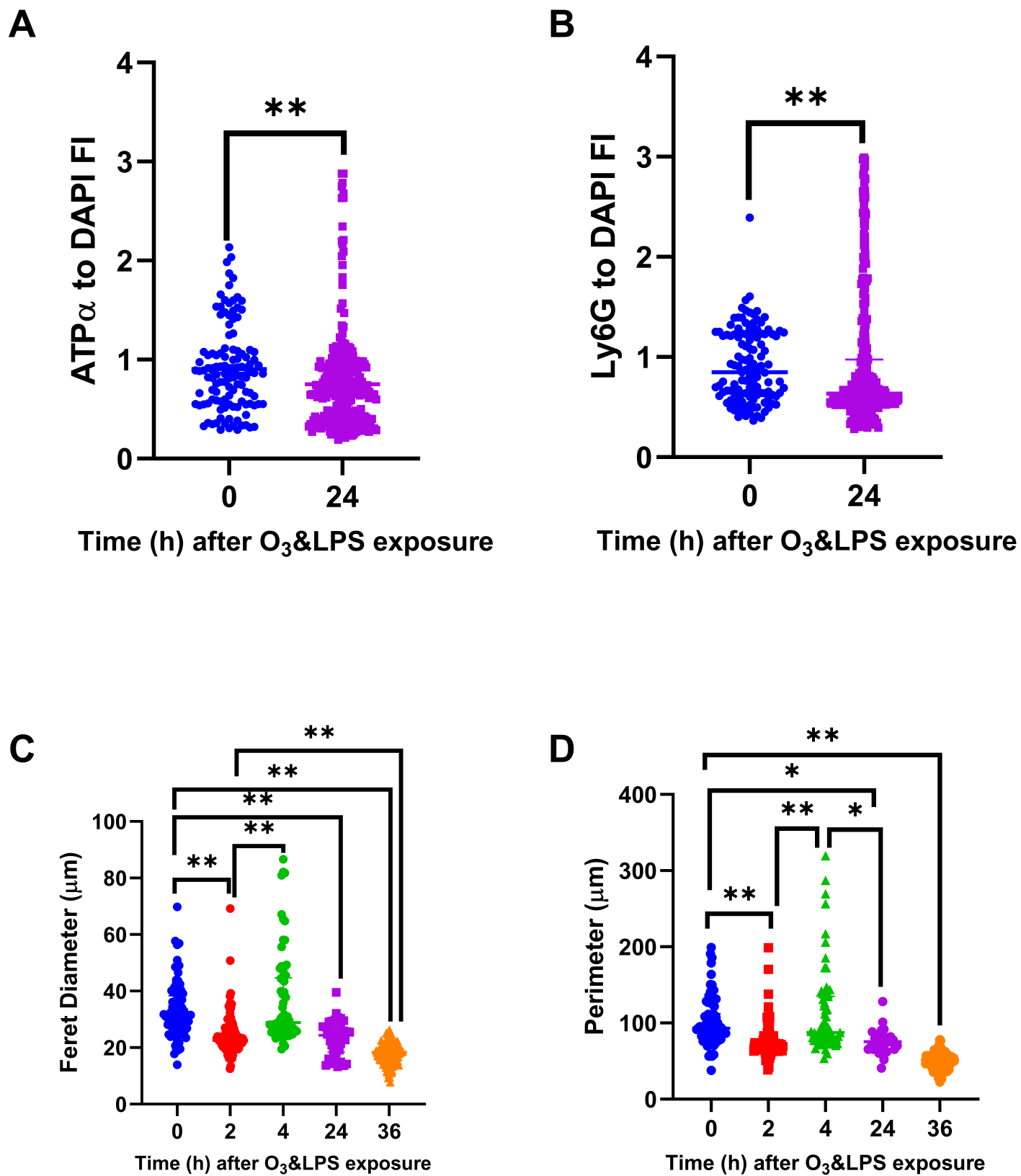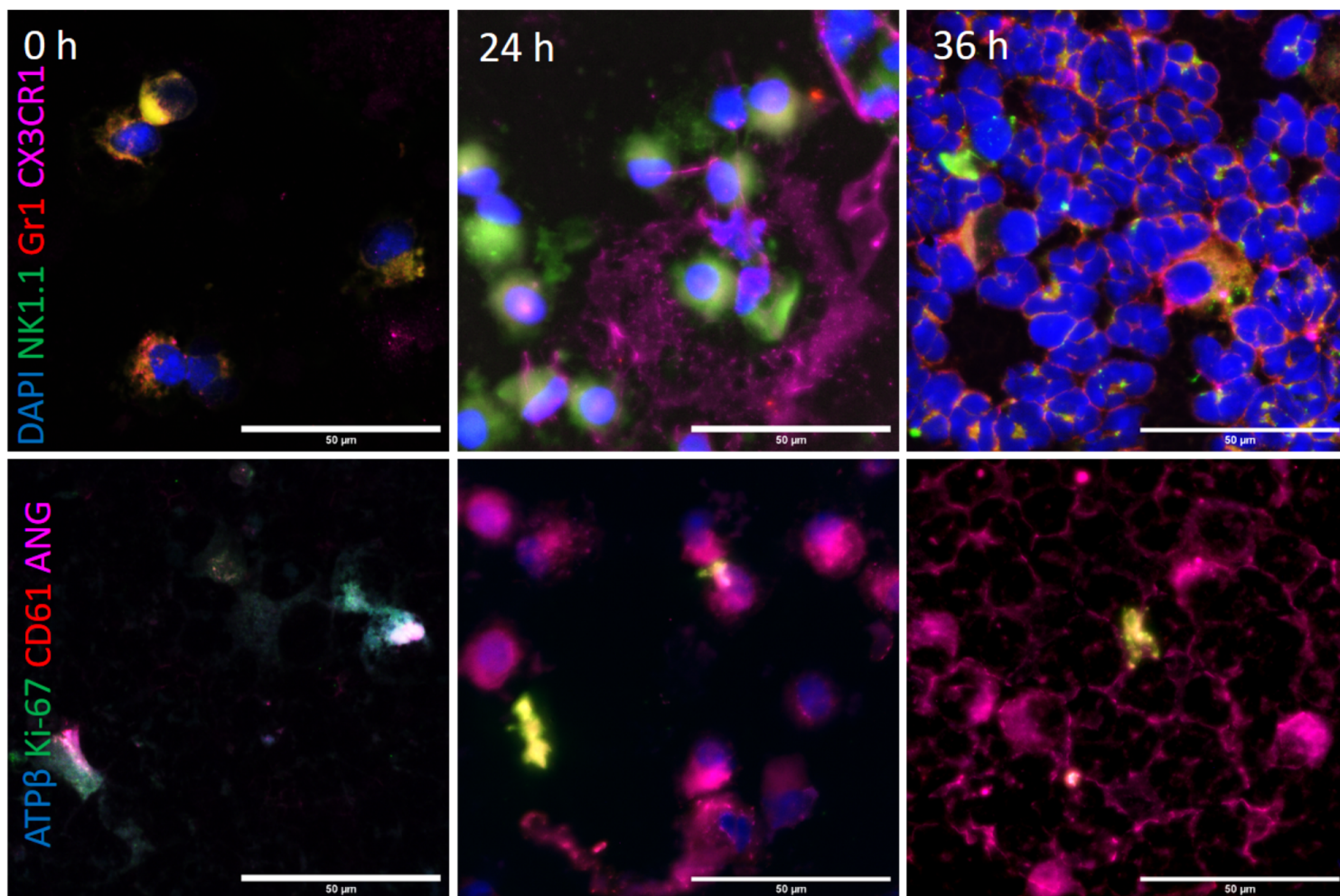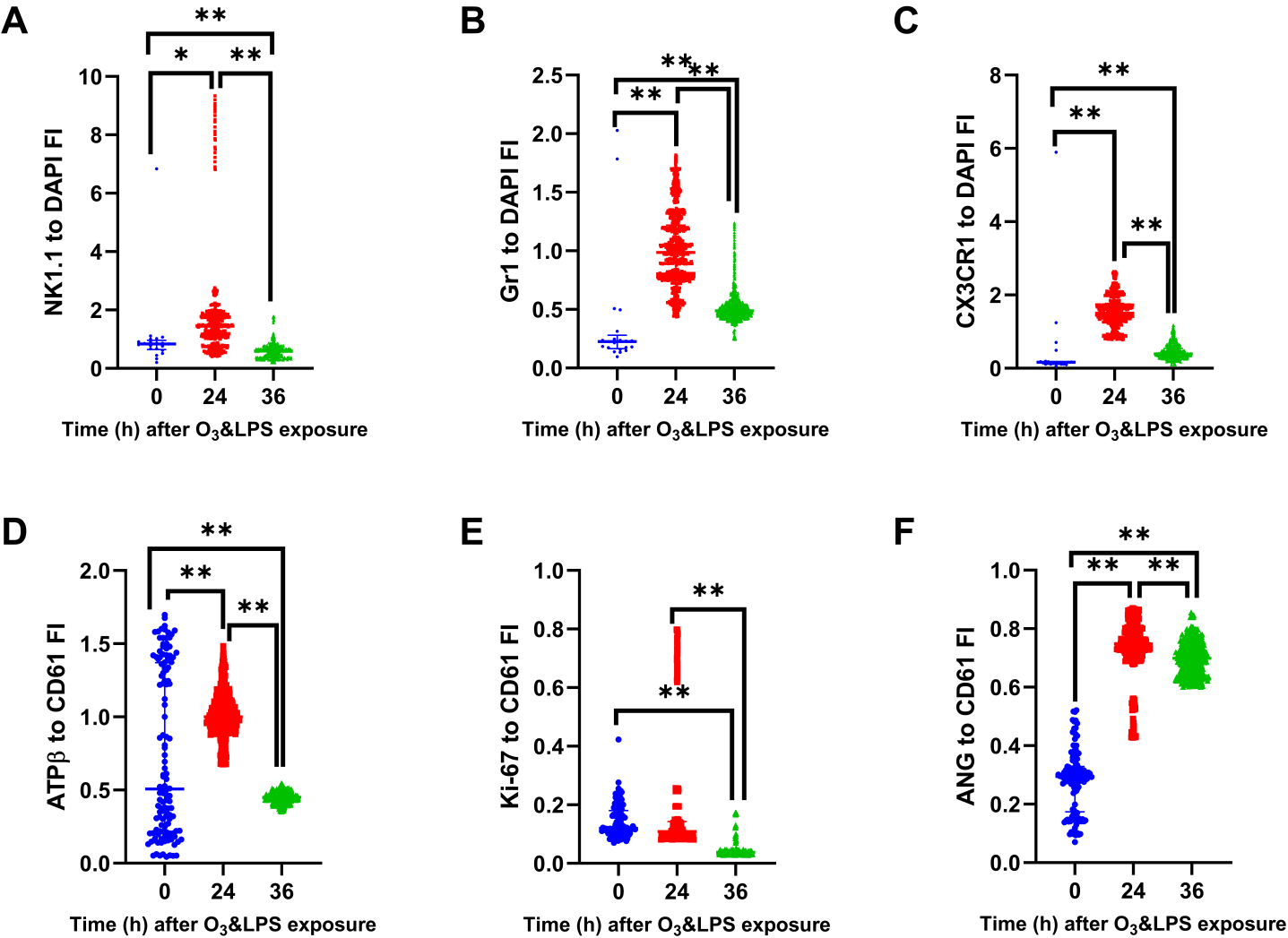
Figure 1

Click here to access/download;Figure;Fig_1.pdf ⬇

A

B

C

D

E

F

24 h

DAPI CX3CR1 Siglec-F

Figure 2

Figure 3

Figure 4

Click here to access/download;Figure;Fig_4.pdf ⬇
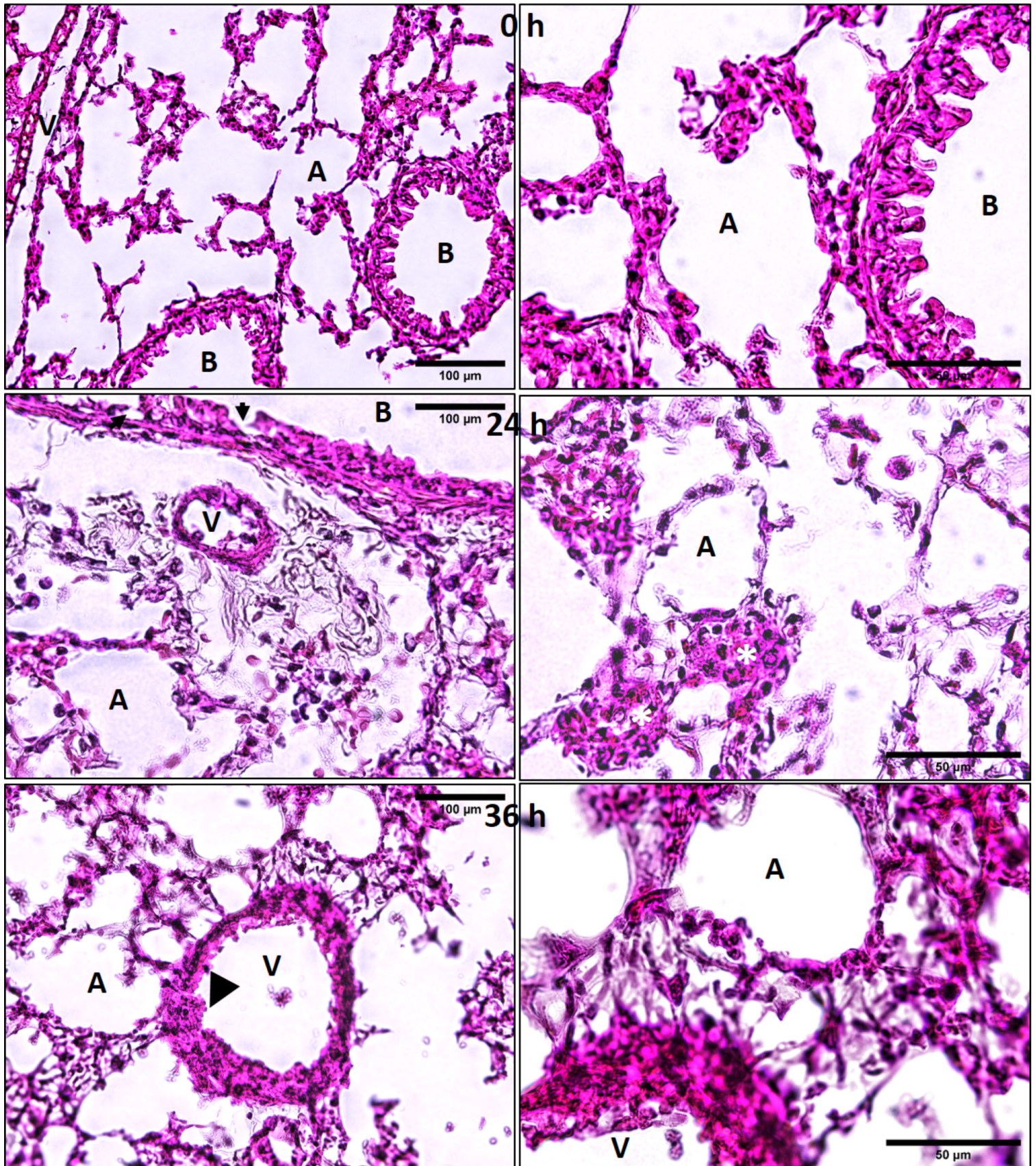
Figure 5

Click here to access/download;Figure;Fig_5.pdf ⬇
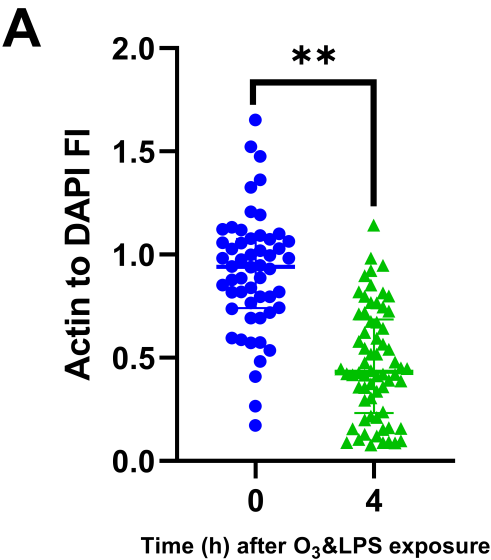
Figure 6

Figure 7

Click here to access/download;Figure;Fig_7.pdf

Figure 8

Figure 9   Click here to access/download;Figure;Fig_9.pdf ±
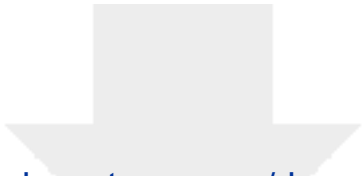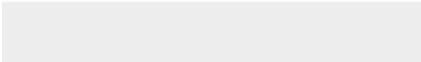
Figure 10
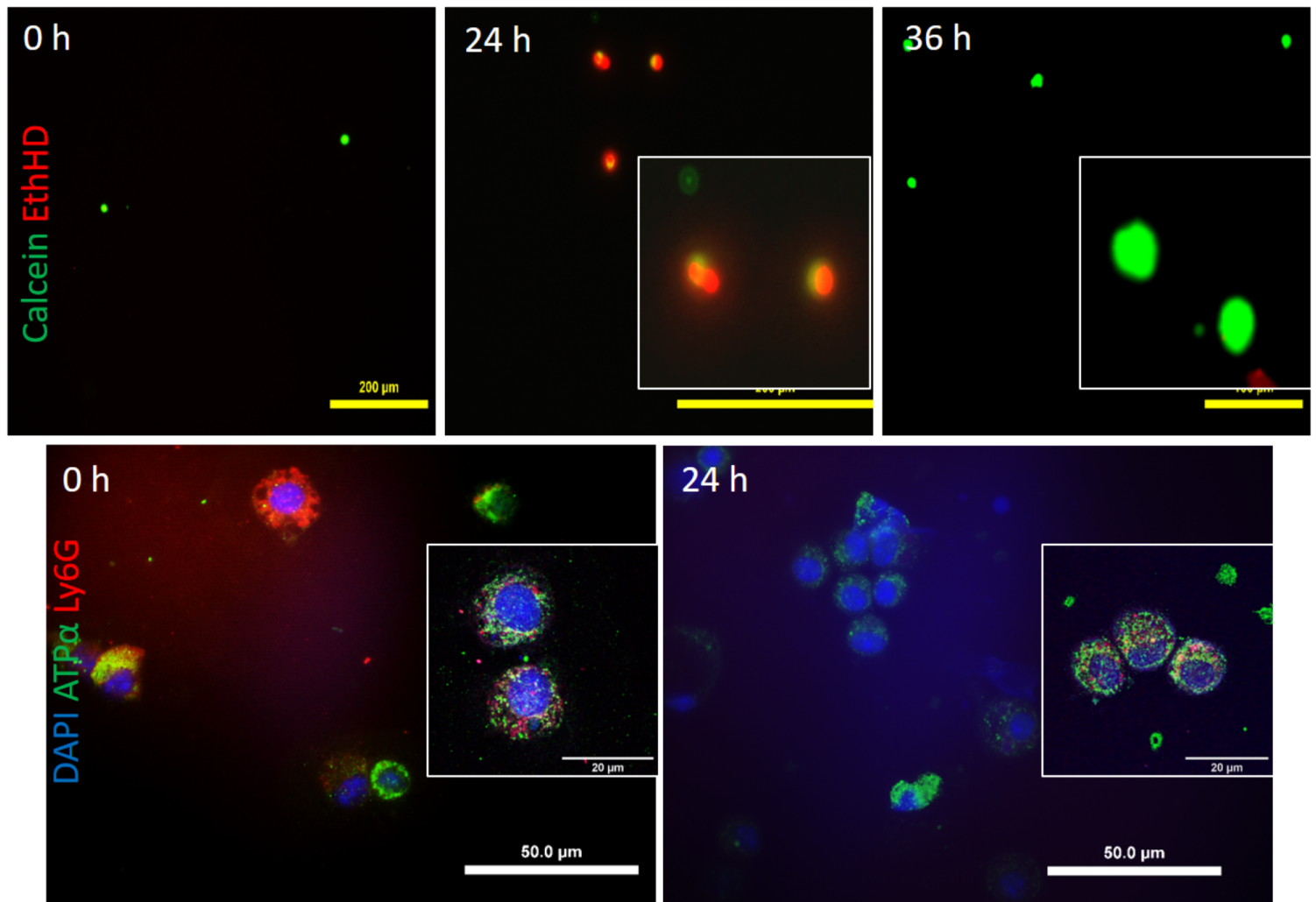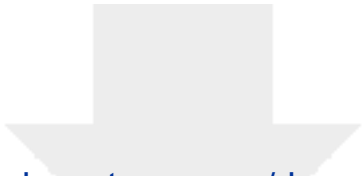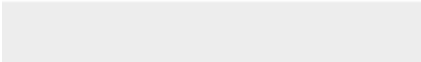
Figure 11

Movie 1

Click here to access/download
Video or Animated Figure
Supp_Movie_1.avi

Click here to access/download
Video or Animated Figure
Supp_Movie_2.avi

S.No.	Primary Antibody	Invitrogen Secondary Antibody
1	Mouse anti-NK1.1 IgG2a kappa (clone PK136), Invitrogen Catalog No. 16-5941-82	Alexa 488 conjugated goat anti-mouse IgG (H+L), Catalog No. A11002
2	Rat anti-Ly6G/Ly6C (Gr1) IgG2b kappa (clone RB6-8C5), Invitrogen Catalog No. 53-5931-82	Alexa 568 conjugated goat anti-rat IgG (H+L), Catalog No. A11077
3	Rabbit anti-CX3CR1 IgG (RRID 467880), Invitrogen Catalog No. 14-6093-81	Alexa 633 conjugated goat anti-rabbit IgG (H+L), Catalog No. A21070
4	Mouse anti-ATP5A1 IgG2b (clone 7H10BD4F9), Invitrogen Catalog No. 459240	Alexa 488 conjugated goat anti-mouse IgG (H+L), Catalog No. A11002
5	Rat anti-Ly6G IgG2a kappa (clone 1A8), Invitrogen Catalog No. 16-9668-82	Alexa 568 conjugated goat anti-rat IgG (H+L), Catalog No. A11077
6	Mouse anti-ATP5β IgG2b (clone 3D5AB1), Thermofisher Catalog No. A-21351	Alexa 350 conjugated goat anti-mouse IgG (H+L), Catalog No. A11045
7	Rat anti-Ki-67 (clone SolA15) IgG2a kappa, Invitrogen Catalog No. 14-5698-82	Alexa 568 conjugated goat anti-rat IgG (H+L), Catalog No. A11077
8	Armenian hamster anti-CD61 (clone 2C9.G2) IgG1 kappa, BD Catalog No. 553343	Alexa 568 conjugated goat anti-hamster IgG (H+L), Catalog No. A21112
9	Rabbit anti-angiostatin (mouse aa 98-116) IgG, Abcam Catalog No. ab2904	Alexa 633 conjugated goat anti-rabbit IgG (H+L), Catalog No. A21070

Read-out	BAL	LVP	PB	SBM	FBM
TLC	*	*	+ at 24 h; - at 36, 72 h		+ at 72 h
Neutrophils	+ at 24, 36, 72 h	+ at 24 h	*	+ at 4, 24, 36, 72 h	+ at 4, 24, 36, 72 h
Protein	+ at 36 h	*	n.d.	n.d.	n.d.
Chemokine profile	- For eotaxin-2, IL-2 at 4, 24, 36, 72 h	+ for Eotaxin-1/2, IL-2, TNFα, IFNγ, CX3CL1, CCL27, IL-16, CXCL5, CXCL10, MIP3β at 4 h; + for SDF1α at 36 h	n.d.	n.d.	n.d.
Cell size	+ at 4 h; - at 24, 36 h	n.d.	n.d.	n.d.	n.d.
ATPα	- at 24 h	n.d.	n.d.	n.d.	n.d.
NK1.1/Ki-67	+ at 24 h	n.d.	n.d.	n.d.	n.d.
ATPβ/Gr1/CX3CR1/ANG	+ at 24, 36 h	n.d.	n.d.	n.d.	n.d.

Name of Material/ Equipment	Company	Catalog Number
33-plex Bioplex chemokine panel	Biorad	12002231
63X oil (NA 1.4-0.6) Microscope objectives	Leica	HCX PL APO CS (11506188)
Alexa 350 conjugated goat anti-mouse IgG (H+L)	Invitrogen	A11045
Alexa 488 conjugated goat anti-mouse IgG (H+L)	Invitrogen	A11002
Alexa 488 conjugated phalloidin	Invitrogen	A12370
Alexa 555 conjugated mouse anti-α tubulin clone DM1A	Millipore	05-829X-555
Alexa 568 conjugated goat anti-hamster IgG (H+L)	Invitrogen	A21112
Alexa 568 conjugated goat anti-rat IgG (H+L)	Invitrogen	A11077
Alexa 633 conjugated goat anti-rabbit IgG (H+L)	Invitrogen	A21070
Armenian hamster anti-CD61 (clone 2C9.G2) IgG1 kappa	BD Pharmingen	553343
C57BL/6 J Mice	Jackson Laboratories	64
Confocal laser scanning microscope	Leica	Leica TCS SP5
DAPI (4′,6-diamidino-2-phenylindole)	Invitrogen	D1306
Inverted fluorescent wide field microscope	Olympus	Olympus IX83
Ketamine (Narketan)	Vetoquinol	100 mg/ml
Live (calcein)/Dead (Ethidium homodimer-1) cytotoxicity kit	Invitrogen	L3224
Mouse anti-ATP5A1 IgG2b (clone 7H10BD4F9)	Invitrogen	459240
Mouse anti-ATP5β IgG2b (clone 3D5AB1)	Invitrogen	A-21351
Mouse anti-NK1.1 IgG2a kappa (clone PK136)	Invitrogen	16-5941-82
Pierce 660 nm protein assay	Thermoscientific	22660
Rabbit anti-angiostatin (mouse aa 98-116) IgG	Abcam	ab2904
Rabbit anti-CX3CR1 IgG (RRID 467880)	Invitrogen	14-6093-81
Rat anti-Ki-67 (clone SolA15) IgG2a kappa	Invitrogen	14-5698-82

Comments/Description
aliquot in 2 µl stocks and store at -20^0C
Dilute 10 times to make a 10 mg/ml stock

February 18, 2021

Dear Dr. Nguyen,

On behalf of my co-authors, please find below our responses (in red font) to the corrections advised. The new video 4.48 minutes in duration. We look forward to your final decision.

Thanks,

Sincerely,

Gurpreet

Changes to be made by the Author(s) regarding the written manuscript:
1. Some minor changes are required for the written manuscript. Please see the comments in the attached manuscript.

All the edits are made and provided in track mode.
2. Please provide Table 1 and 2 as xls/xlsx files.

Please find the excel file with 2 separate sheets with Tables 1 and 2.

Changes to be made by the Author(s) regarding the written manuscript:
1. Please provide on screen graphics with the speakers' names and institutions in the intro. Please refilm the intro with the second speaker to avoid vertical video. Corrected
2. Please increase the speakers audio in the beginning, it is too quiet. Done